

Drew University

College of Liberal Arts

Ca²⁺ Catalyzed Adenosine 3', 5'-Cyclic Monophosphate Hydrolysis: Insights into the
Role of Metals in Phosphodiesterase Active Sites

A Thesis in Biochemistry and Molecular Biology

by

Julie Alex

Submitting in Partial Fulfillment

of the Requirements

for the Degree of

Bachelor in Arts

With Specialized Honors in Biochemistry and Molecular Biology

April 2018

Abstract

Cyclic adenosine monophosphate (cAMP) is an important secondary messenger found within biological systems. A family of phosphodiesterases (PDEs) hydrolyze cAMP into 5' adenosine monophosphate which is further processed into adenosine to alter signaling pathways. PDEs have been a pharmaceutical target for diseases, including end-stage heart failure, autoimmune diseases/allergies, and contractile dysfunction, that are impacted by extreme cAMP fluxes. A new model system using calcium (Ca^{2+}) was analyzed for the production of 3'AMP and 5'AMP along with the mechanism of metal ion catalysis. In this study, kinetic assays with high pressure liquid chromatography were used with Ca^{2+} ions and cAMP to collect rate constants, and to conduct product and reactant analysis. The products were confirmed to be 3'AMP and 5'AMP using electrospray ionisation time-of-flight (ESI-TOF) mass spectroscopy and comparison with HPLC standards. The current model system shows an increase in the ratio of 3'AMP versus 5'AMP production as $[\text{Ca}^{2+}]$ increase. Once rate constants were collected, they were compared with the current DNA and RNA models. Graphing the rate constants versus Ca^{2+} concentration shows a second order curve fit similar to the DNA model, p-nitrophenyl-thymidine- 5'-phosphate (T5PNP), and different to the RNA model. The k_0 with no Ca^{2+} is $2.6 \cdot 10^{-4} \text{ s}^{-1}$, $k_{1\text{st}}$ with 1st order Ca^{2+} is $1.6 \cdot 10^{-2} \text{ M}^{-1} \text{ s}^{-1}$, and $k_{2\text{nd}}$ with 2nd order Ca^{2+} is $2.3 \cdot 10^{-1} \text{ M}^{-2} \text{ s}^{-1}$ for the pseudo-first order reaction in regards to Ca^{2+} . When analyzing the difference in catalysis of NaOH and Ca^{2+} , the $\Delta\Delta G^\ddagger$, difference in activation energy stabilization, is 18 kJ/mol. Isotope reactions with alkaline phosphatase indicate that the hydroxide attacks the phosphorus instead of the carbon. This model system allows for intermediate analysis to determine a dual ion mechanism and attack at the phosphorus.

TABLE OF CONTENTS

Abstract	
Table of Contents	
List of Figures	
Introduction	1
Biological Role of Cyclic Adenosine Monophosphate.....	1
Phosphodiesterase as Pharmaceutical Target.....	5
Enzymatic Catalysis: Phosphodiesterase.....	6
Phosphoesters and Phosphoryl Transfer.....	10
Metal Ion Catalysis.....	16
Model Systems.....	17
Current Work.....	24
Methods	29
Kinetic Assays.....	29
Isotope Assays.....	31
Results	32
Discussion	54
Model System Analysis.....	54
Comparison with DNA and RNA Models.....	57
Product Ratio Analysis.....	59
Isotope Analysis.....	60
Future Directions.....	61
Conclusion.....	62
References	64

List of Figures

- Figure 1: Protein Kinase A Pathway
Figure 2: Cyclic Adenosine Monophosphate Structure
Figure 3: The Energy Diagram for an Enzyme Catalyzed versus not Catalyzed
Figure 4: Stick and Ball Representation of the Active Site of PDE 4 with cAMP as the Substrate
Figure 5: Molecular Representation of Phosphomonoester, Phosphodiester, and Phosphotriesters
Figure 6: Molecular Representations of the Three Different Transition States
Figure 7: Magnified Model of DNA Showing Phosphodiester Linkage
Figure 8: Metal Ion Catalysis Methods of cAMP
Figure 9: RNA versus DNA Model Hydrolysis
Figure 10: Secondary Plots to Differentiate Metal Ion Mechanisms
Figure 11: Cobalt Metal Ion Model System Reaction Scheme
Figure 12: Attack at Phosphorus Versus Carbon
Figure 13: Isotope Assay Reaction Scheme
Figure 14: HPLC Chromatographs of Standards and Reaction
Figure 15: HPLC Chromatograph of 0.33 M CaCl₂ Reaction at 33 Hours
Figure 16: HPLC Chromatographs of Control Experiment
Figure 17: Chromatograph Analysis of 0.33 M CaCl₂ Reaction with cAMP
Figure 18: Mass Spectrometry Analysis of 0.33M CaCl₂ Reaction with cAMP using ESI-TOF Method
Figure 19: Change in Mole Percentage Over Time for a 0.33 M CaCl₂ Reaction with cAMP
Figure 20: Chromatograph of 1 M NaOH Reaction with cAMP and Adenosine Standard
Figure 21: Change in Mole Percentage Over Time for a NaOH Reaction with cAMP
Figure 22: Rate Constant for cAMP Versus [Ca²⁺].
Figure 23: Rate Constant Versus [Ca²⁺] at Lower pH
Figure 24: Ca²⁺ Influences the Product Ratio of cAMP Hydrolysis
Figure 25: ESI-TOF method mass spectroscopy of ¹⁸O isotope incorporated 3' and 5'AMP
Figure 26: ESI-TOF method mass spectroscopy of Adenosine Derived from ¹⁸O isotope incorporated 5'AMP and 3'AMP
Figure 27: Proposed Reaction Scheme of NaOH Catalyzed Hydrolysis of cAMP
Figure 28: Proposed Reaction of Ca²⁺ Catalyzed Hydrolysis

List of Tables

- Table 1: Calculated $\Delta\Delta G^\ddagger$ of Ca²⁺ Catalyzed versus NaOH
Table 2: Fold Catalysis Comparison Between Model Systems

Introduction

Biological Role of Cyclic Adenosine Monophosphate

Communication and synchronization between organs within the body are required for physiological processes to function properly. An example of this communication is when endocrine glands release hormones to alert cells about metabolic processes needed to maintain homeostasis through signaling pathways. Primary messengers are released to initiate pathways, usually acting as an external influence on the cell to continue a cascade within the cell. The intracellular part of the signal can be controlled by secondary messengers, such as cyclic adenosine monophosphate (cAMP). The primary messenger molecules can use the protein kinase A pathway to start the cascade. Prostaglandins, histamine, β -adrenergic agonists, β -endorphin, adenosine, and neuropeptide hormones are primary messengers that cause effector T cells to synthesize high concentrations of cAMP, which inhibits proliferation of naturally occurring regulatory T cells (Wehbi and Taskén 2016, Bopp et al. 2007). However, cAMP also participates in multiple pathways that regulate bodily systems, such as metabolism and immune system function (Serezani et al. 2008).

Signaling pathways that activate cAMP production begins with a heterotrimeric G-protein (Serezani et al. 2008). The primary messenger production will bind causing the release of the alpha subunit of the heterotrimeric G-protein (Figure 1). This stimulation will cause an exchange in a guanosine diphosphate (GDP) for guanosine triphosphate (GTP) on the alpha subunit. This change allows the alpha subunit to detach from the beta subunit.

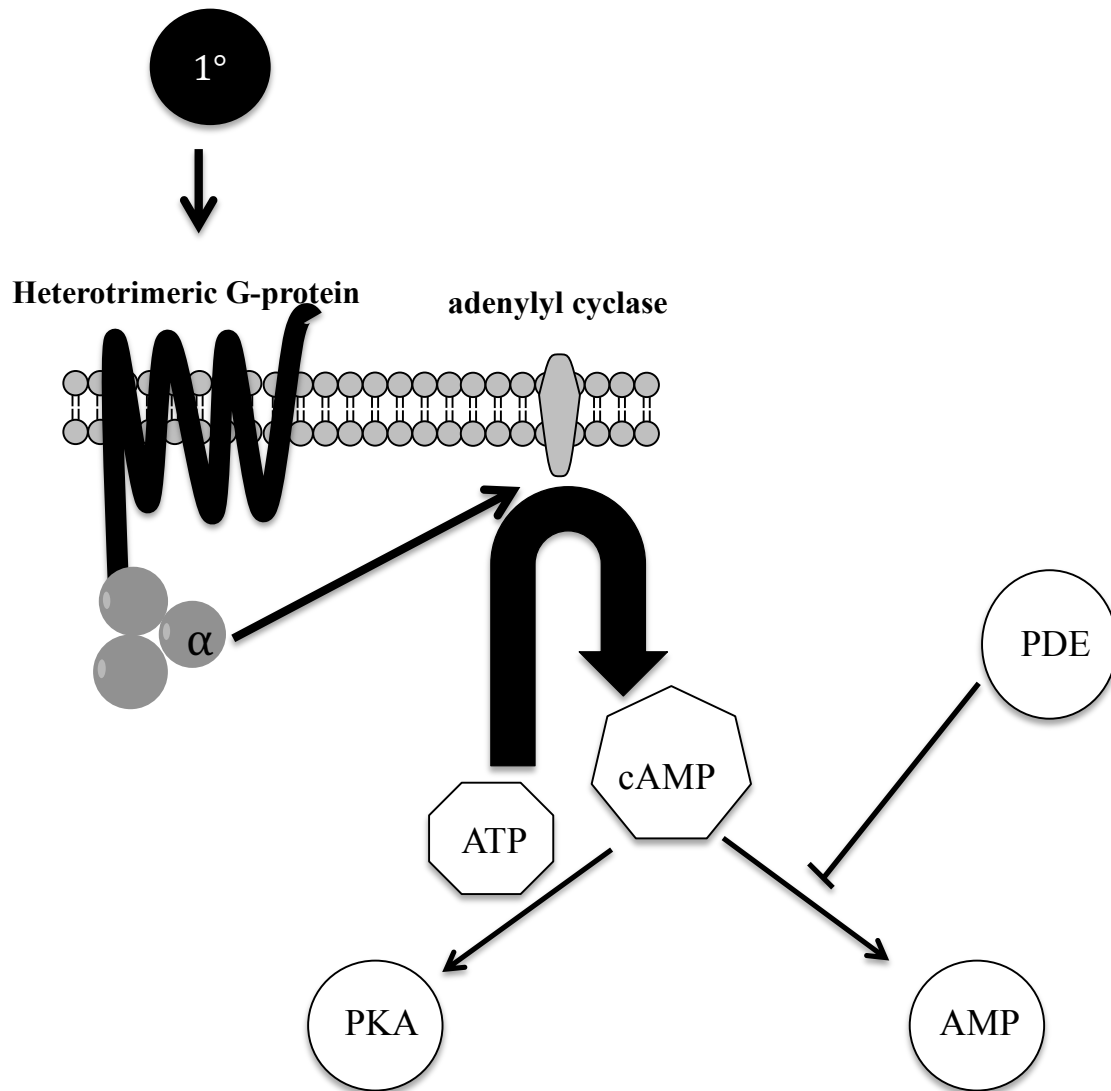


Figure 1. Protein Kinase A Pathway. Multiple primary messengers (1°), including chemokines and hormones such as epinephrine, activate cAMP by binding to a heterotrimeric G- protein. The binding causes the release of the alpha subunit which activates adenylyl cyclase to synthesize cAMP. cAMP activates protein kinase A (PKA) through binding. Phosphodiesterases (PDE) will degrade cAMP into AMP to stop the PKA pathway.

The alpha subunit can then activate adenylyl cyclase to turn adenosine triphosphate (ATP) into cAMP, with pyrophosphate forming as a side product. Once cAMP is produced, it can activate protein kinase A (PKA) by binding to the regulatory subunits. PKA phosphorylates other enzymes in order to activate them. This pathway can activate many important biological functions such as metabolism, immune function, and insulin secretion (Soderling and Beavo 2000).

Cyclic AMP and PKA play an important role in human health. Some pathogens are able to control immune function by being able to act on the alpha subunit of the G-protein to cause a shift in cAMP production. Additionally, many autoimmune diseases can form when there is an imbalance of cAMP, and thus homeostasis is no longer maintained. Diseases such as chronic infections and cancer can take advantage of PKA pathway and increase the concentration of cAMP so that immune function can be inhibited (Serezani et al. 2008). Certain clinical states cause higher concentrations of cAMP including human immunodeficiency virus infection, smoking, chronic obstructive pulmonary disease, bone marrow transplant, infancy, aging, burns, malnutrition, and cystic fibrosis (Serezani et al. 2008).

Bacteria also take advantage that high concentrations of cAMP interrupts immune system function. Bacteria produce a high concentration of cAMP to secrete into its surroundings while in the host (Buettner et al. 1973). Pathogens can also indirectly cause their host to produce cAMP by releasing primary messengers, such as histamine, from within the host's paracrine and autocrine system (Serezani et al. 2008). This strategy can be used to combat environmental stressors that can affect the bacteria as well. An

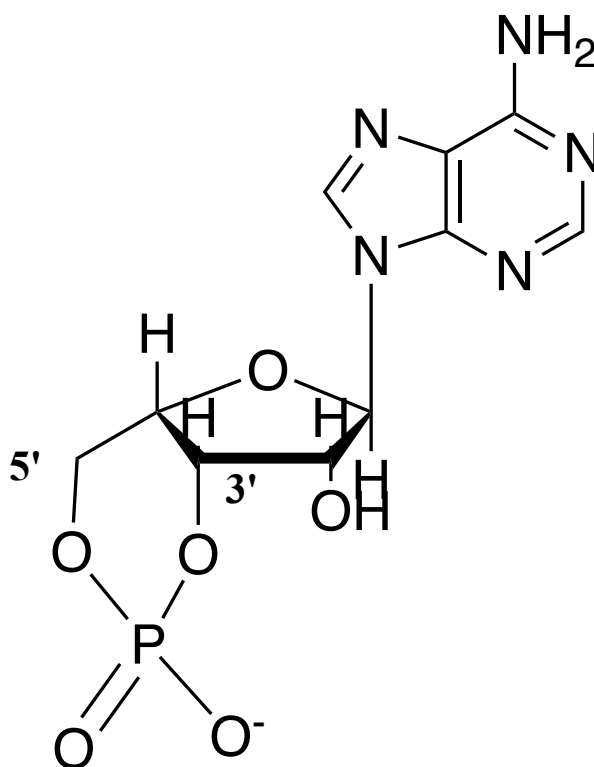


Figure 2. Cyclic Adenosine Monophosphate Structure. The adenosine is attached to the cyclized monophosphate, creating a phosphodiester. The 5' and 3' positions are labeled to show points of cyclization.

example of this is when glucose levels are low, bacteria increase cAMP production in themselves to start the pathway that eventually causes an increase in lac operon transcription (Serezani et al. 2008). Due to these survival strategies, bacteria could inhabit human bodies and multiply without being attacked by the immune system. Understanding the mechanism of controlling cAMP levels may help in defending against such inhabitations. This will include production and cleavage of cAMP; this paper's focus will be on degradation. cAMP is made up of an adenosine with a monophosphate that has been cyclized at the 5' and 3' positions and for degradation there must be cleavage of the phosphodiester bond (Figure 2). This is conducted by a family of phosphodiesterases (PDEs) within the body.

Phosphodiesterase as Pharmaceutical Targets

As homeostasis is required for general health, diminished cAMP can also be harmful to organisms, which can be combatted through drugs. Specific diseases related to cAMP deficiencies are contractile dysfunction, autoimmune disorders, allergies, and end-stage heart failure (Feldman et al. 1987). There are multiple treatments for these disturbances caused by a lack of homeostasis. Non-steroidal inflammatory drugs have been predominantly used to increase the cAMP concentrations. PDE inhibitors, beta adrenergic receptor agonists, prostaglandin E2 analogs, and prostaglandin I2 (prostacylin) analogs combat diseases caused by a lack of cAMP (Serezani et al. 2008).

PDEs have been the target of many pharmaceutical companies due to the many systems in which cAMP is involved. There are multiple PDEs which are categorized numerically. For the past fifty-seven years, eleven families of PDEs have been identified

and their specificities have been studied (Halpin 2008, Nichol森 et al. 1991); each PDE has been studied to analyze its specificity for substrates to cater more towards cAMP or towards cyclic guanosine monophosphate (cGMP). There are a variety of tissues where these enzymes and their multiple isoforms can be found. For example the PDE5 enzyme found in nervous tissue has been a specific pharmacological target since it plays a role in erectile dysfunction (Corbin and Francis 2002, Ariano and Appleman 1979). Drug research has allowed for the production of multiple medications such as IBMX, sildenafil, zaprinast, and tadalafil to inhibit PDE5 (Carter et al. 1998).

PDE4 inhibitors have been found to have anti-inflammatory activity. This is an innovative method in which chronic obstructive pulmonary disease (COPD) can be treated because glucocorticosteroids have been failing as anti-inflammatories (Hamblin et al. 2008). Through high-throughput screening, X-ray crystallography, and rat pharmacokinetic assays, pyrazolopyridines have been found as highly specific inhibitors of PDE4 (Hamblin et al. 2008). Another PDE4 inhibitor, crisaborole ointment, is an approved treatment for atopic dermatitis, also known as eczema (Paller et al. 2016). These different PDE inhibitors allow for alternate pathways than glucocorticosteroids to treat highly prevalent diseases such as COPD and eczema.

Enzymatic Catalysis: Phosphodiesterase

Biological systems can use enzymes to catalyze the hydrolysis or cleavage of phosphodiester bonds. Enzymes use many different methods to shorten reaction time by lowering the activation energy as seen in Figure 3 (Schramm 1998). This stabilization is

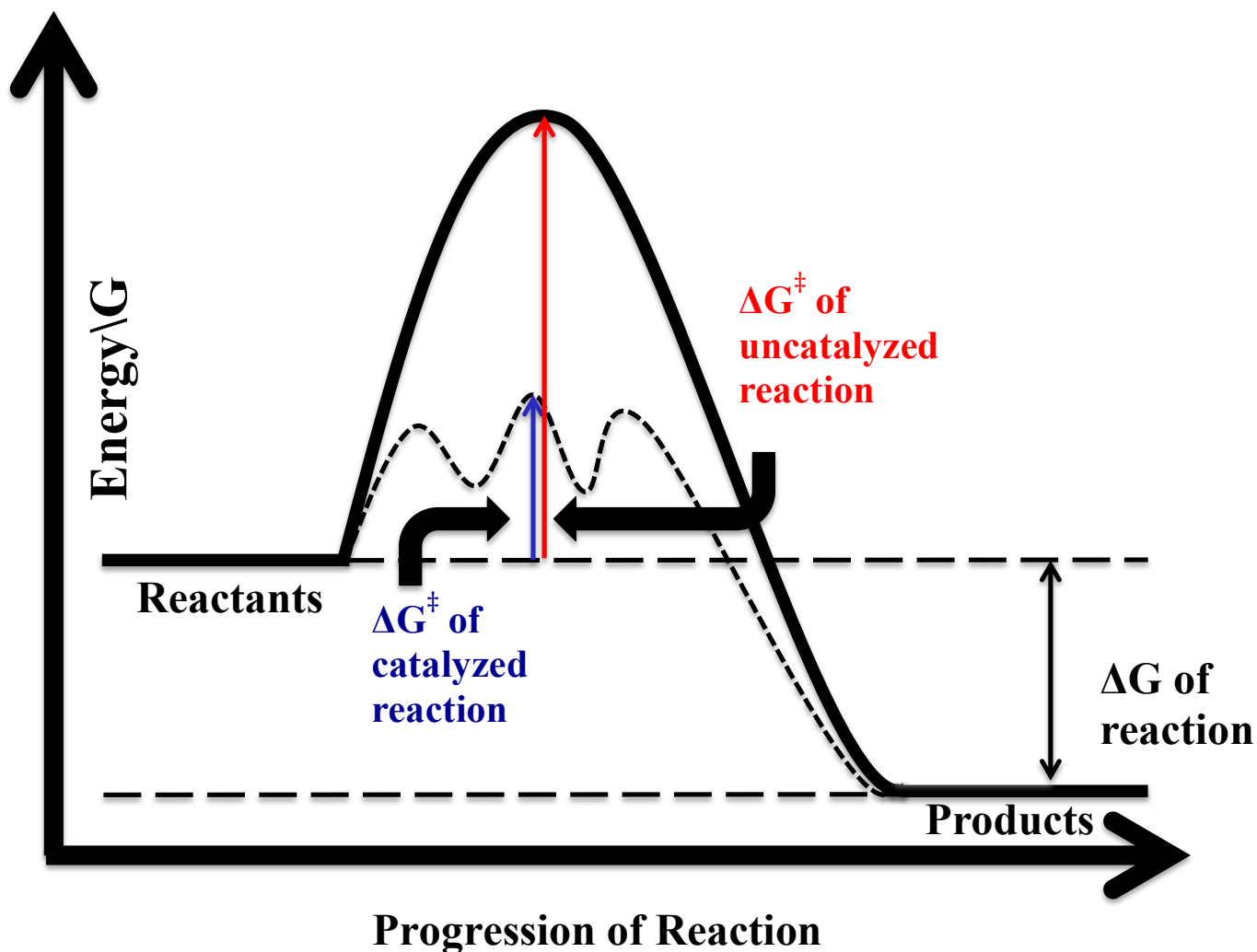


Figure 3. The Energy Diagram for an Enzyme Catalyzed versus not Catalyzed. The delta G (ΔG) of the reaction is the difference in energy between the reactants and the products. The smaller delta G^\ddagger of activation is shown for the catalyzed reaction plot in blue versus the larger delta G^\ddagger of activation for the uncatalyzed reaction plot in red.

necessary since cAMP is kinetically stable due to the phosphodiester bond. Enzymatic catalysis can amplify or decrease signals of multiple biological mechanisms due to the production or degradation of cAMP. For example, it is necessary in neurons where sometimes within milliseconds the cAMP levels need to shift from high concentrations to low concentrations due to neuronal stimuli (Breer and Shepherd 1993). PDEs are able to take advantage that phosphodiesterases are kinetically stable but thermodynamically unstable, which will be expanded upon later.

Enzymes, in general, are able to create an environment in which the energy needed for the transformation is lowered and more favorable for attack. Enzymes can use multiple amino acid residues, water molecules, and metal ions position to stabilize the transition state of the reaction and increase rate of catalysis. Families of PDEs catalyze the hydrolysis of cAMP with approximately a 10^{17} fold enhancement shown through kinetics studies (Schroeder et al. 2006). The half-life of cAMP was calculated to be 732,000 years; however, within an enzyme active site, the half-life for cAMP is 0.1 milliseconds (Chin and Zhou 1987). This type of environment also allows for maintenance of specificity (Fersht 1999). Crystallization of PDE4 with AMP bound to the active site gave insight into the binding of the metal ions to the other portions of the active site (Figure 4 adapted from Huai et al. 2003). Based on the crystal structure, water molecules, metal ions, and amino acid residues coordinate with cAMP within the active site to catalyze hydrolysis. Specifically, two metal ions coordinate therefore a binuclear mechanism is used. A nucleophile is a molecule that donates electrons to another

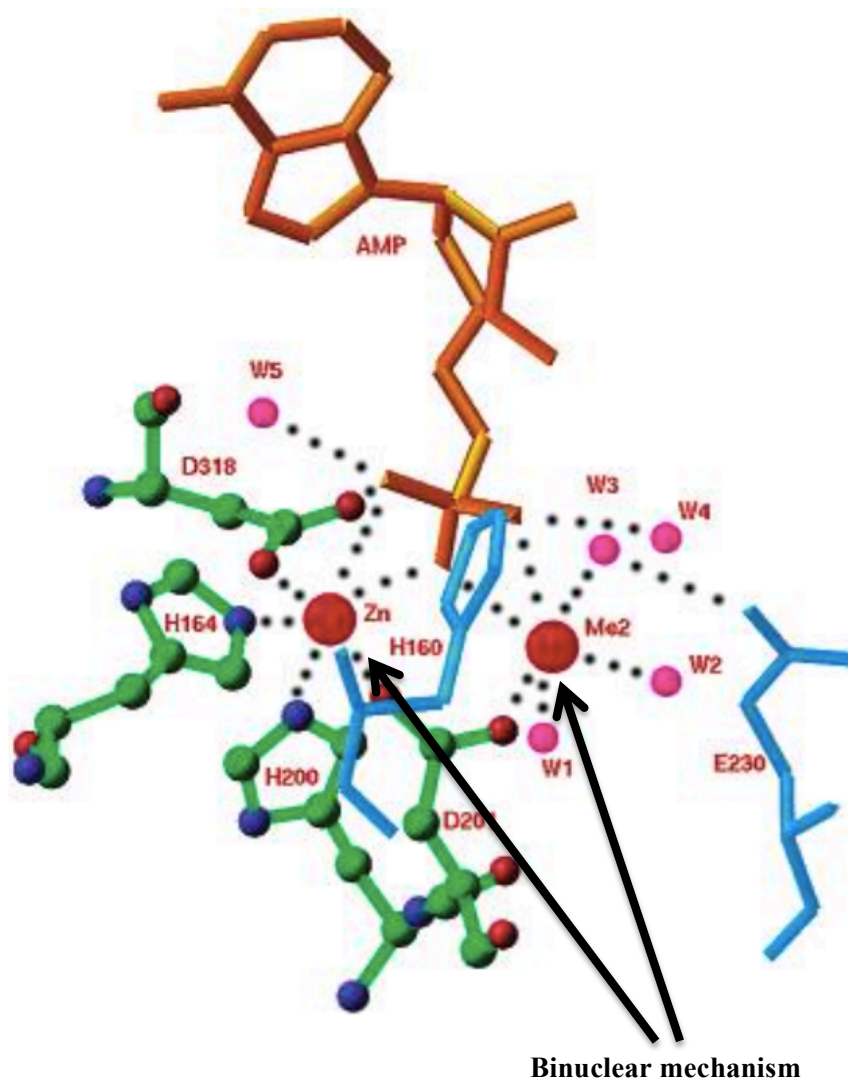


Figure 4. Stick and Ball Representation of the Active Site of PDE 4 with cAMP as the Substrate. The red balls represent the zinc ions coordinating with the water molecules (pink circles W1 to W5), cAMP (orange stick structure), and amino acid residues (green or blue ball and stick structures). The black arrows show the binuclear mechanism due to two zinc atoms being coordinated within the active site. Dotted lines indicate non-covalent interactions. Figure adapted from Huai and colleagues 2003.

molecule, the electrophile, for the creation of a bond. Also, coordination with the phosphate supports nucleophilic attack at the phosphorus atom.

Although the crystal structure gives insight to coordination and information about positioning and interaction, it gives little information on the specific catalytic contribution of each part within the active site. Thus, the relative energy contributions of the three contributing factors of hydrolysis, water, metal ions, and the residues cannot be differentiated. Assessing the catalysis of metal ions requires a model system that separates out the activity of the metal ions. Therefore, a baseline of what these metal ions exactly do to catalyze the hydrolysis of cAMP would be useful along with expanding phosphodiester knowledge.

Phosphoesters and Phosphoryl Transfer

Understanding the catalytic abilities of phosphodiesterases in phosphoryl transfer can aid in drug development. Phosphoryl transfer is the process by which phosphoesters are degraded and synthesized. Phosphates can exist as monoesters, diesters, or triesters (Figure 5). Each phosphoester serves a purpose based on the function that the structure allows; for example, phosphodiesters are integral to genetic material, RNA and DNA. In addition, phosphodiesters also have a role as secondary messengers (Lasilla et al. 2011). Examining the three phosphoesters allow for a good comparison between them.

Phosphomonoesters and phosphotriesters are more reactive than phosphodiesters due to their inherent structures (Figure 5) (Lasilla et al. 2011). Phosphomonoesters have a negatively charged leaving group, [OR]⁻, that is repelled by electron density on the non-

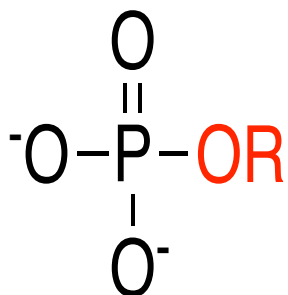
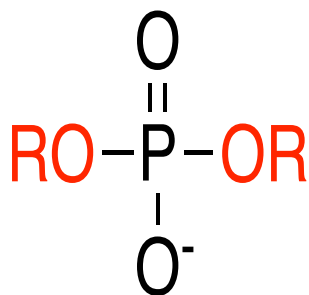
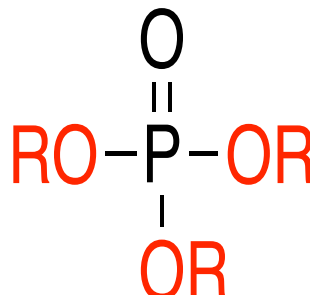
Phosphomonoester**Phosphodiester****Phosphotriester**

Figure 5. Molecular Representation of Phosphomonoester, Phosphodiester, and Phosphotriesters. Phosphomonoesters contain one bridging oxygen atom, phosphodiester contains two bridging oxygen atoms, while phosphotriesters contain three bridging oxygen atoms. Bridging oxygens are highlighted in red and R represents side chains. The remaining oxygen atoms are termed "non-bridging" oxygen atoms, since they only have one bond, and any negative charge is shared equally among these atoms.

bridging oxygen atoms thus speeding up the rate of hydrolysis (Bunton et al. 1958).

Phosphotriesters are more susceptible to nucleophilic attack considering that there is no negative charge to repel nucleophile from attacking the phosphate atom. On account of the lack of negative charge on the other groups, electrostatic repulsion is reduced. Thus, monoesters and triesters have faster reaction rates for phosphoryl transfer.

Phosphoryl transfer cleaves the phosphorus and bridging oxygen bond to create a new phosphorus-oxygen bond through nucleophilic attack. Studies suggest a concerted mechanism by which monoesters go through a phosphoryl transfer where the nucleophilic attack and leaving group leaves at the relatively same time (Lasilla et al. 2011). This can be generally applied to other phosphoesters with good leaving groups. However, the three types of phosphoesters differ in their transition states according to both kinetic isotope effect (KIE) data and linear free energy relationships (LFER) analysis of transition state structure (Lasilla et al. 2011). The results showed that phosphomonoesters go through a loose transition state, in which bond breakage of leaving group predominates over bond formation with nucleophile. Phosphotriesters have a tight transition state, meaning bond formation is more predominant than bond breakage. As may be expected, phosphodiester have a synchronous transition state in between the two types of esters. The three different transition states are shown in Figure 6. In sum, phosphoryl transfer is concerted for phosphoesters with good leaving groups; however, there are distinctions between the monoester, diester, and triester.

There are also other differences that set apart phosphodiester containing molecules. Aside from the differences in transition states due to electrostatic interactions,

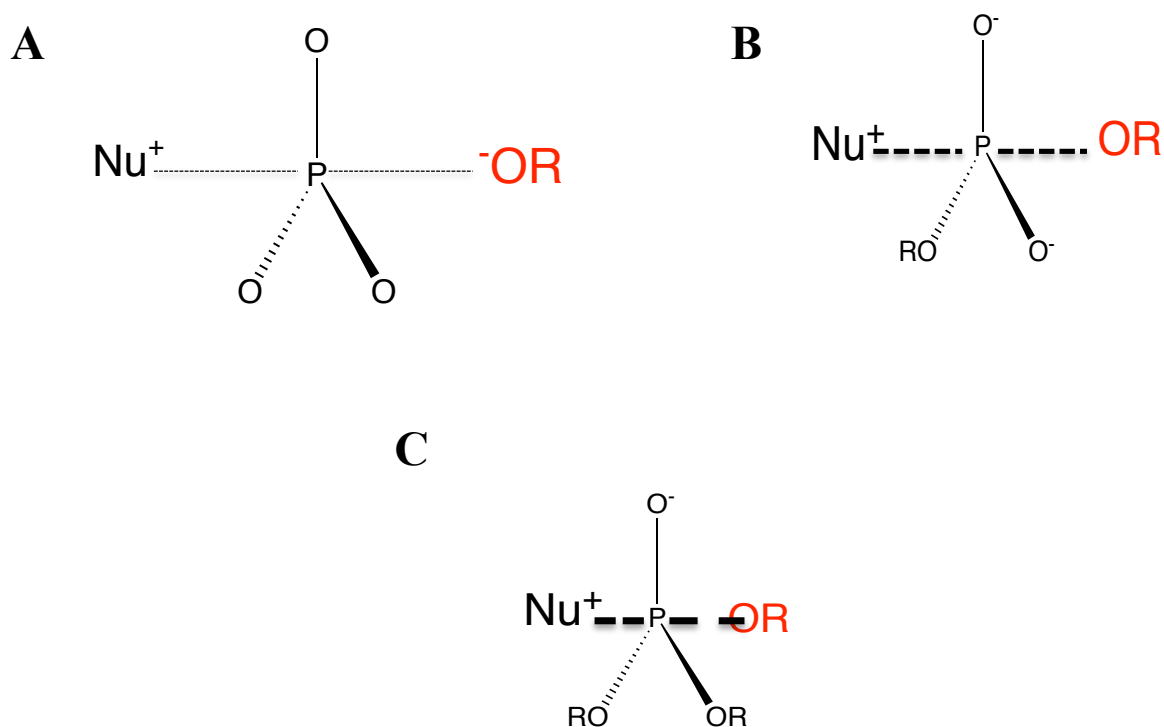


Figure 6. Molecular Representations of the Three Different Transition States.

Side chains are represented by R. **A.** Loose transition state with nucleophile (Nu) and the leaving group OR (red). Bond cleavage is more predominant than nucleophilic attack for phosphomonoesters which is shown by the thinner and longer dashed line. **B.**

Synchronous transition state is where nucleophilic attack and bond cleavage advance at a similar rate for phosphodiester, as shown by the slightly thicker and shorter dashed line that that of phosphomonoester cleavage. **C.** Tight transition state is where nucleophilic attack happens at a faster rate than bond cleavage for phosphotriester, which is shown by the slightly thicker and shorter dashed line that that of phosphodiester cleavage.

other limiting factors such as poor leaving groups, such as alkoxides (Williams and Wyman 2001). Deoxyribonucleic acid (DNA), ribonucleic acid (RNA), and multiple secondary messenger molecules contain phosphate bonds. Having stable bonds is a necessity for biological function because it allows for stable compounds that can only be broken down in certain controlled environments.

Phosphodiester bonds are integral to biological systems by granting great stability to DNA, RNA, secondary messengers, and other physiological existing molecules (Westheimer 1987). Phosphodiester bonds allow certain molecules to be prevalent within biology. The negative charge from the phosphate in the backbone serves multiple purposes in biological molecules. One is that charges will deter molecules from passing through a lipophilic membrane (Westheimer 1987). The electron density on the phosphate also deters any nucleophile from attacking due to electron repulsion (Lasilla et al. 2011). The surrounding electronegative oxygen atoms, and especially the negatively charged oxygen atom, prevent hydroxyl groups from attacking the electrophilic phosphorus atom. Reducing the likeliness of attack contributes to the low reactivity of the molecule.

The most prevalent and well known of the phosphodiester bonds are in DNA in which the nucleotides in the single strands are connected through phosphodiester linkages (Figure 7). This negatively charged backbone prevents nucleophilic attack and therefore genetic material degradation. In addition to providing stability in nucleic acids, phosphodiester bonds also play a prominent role within signaling molecules. Signaling can allow the activation of transcription to occur. An example of that is cAMP acts as a

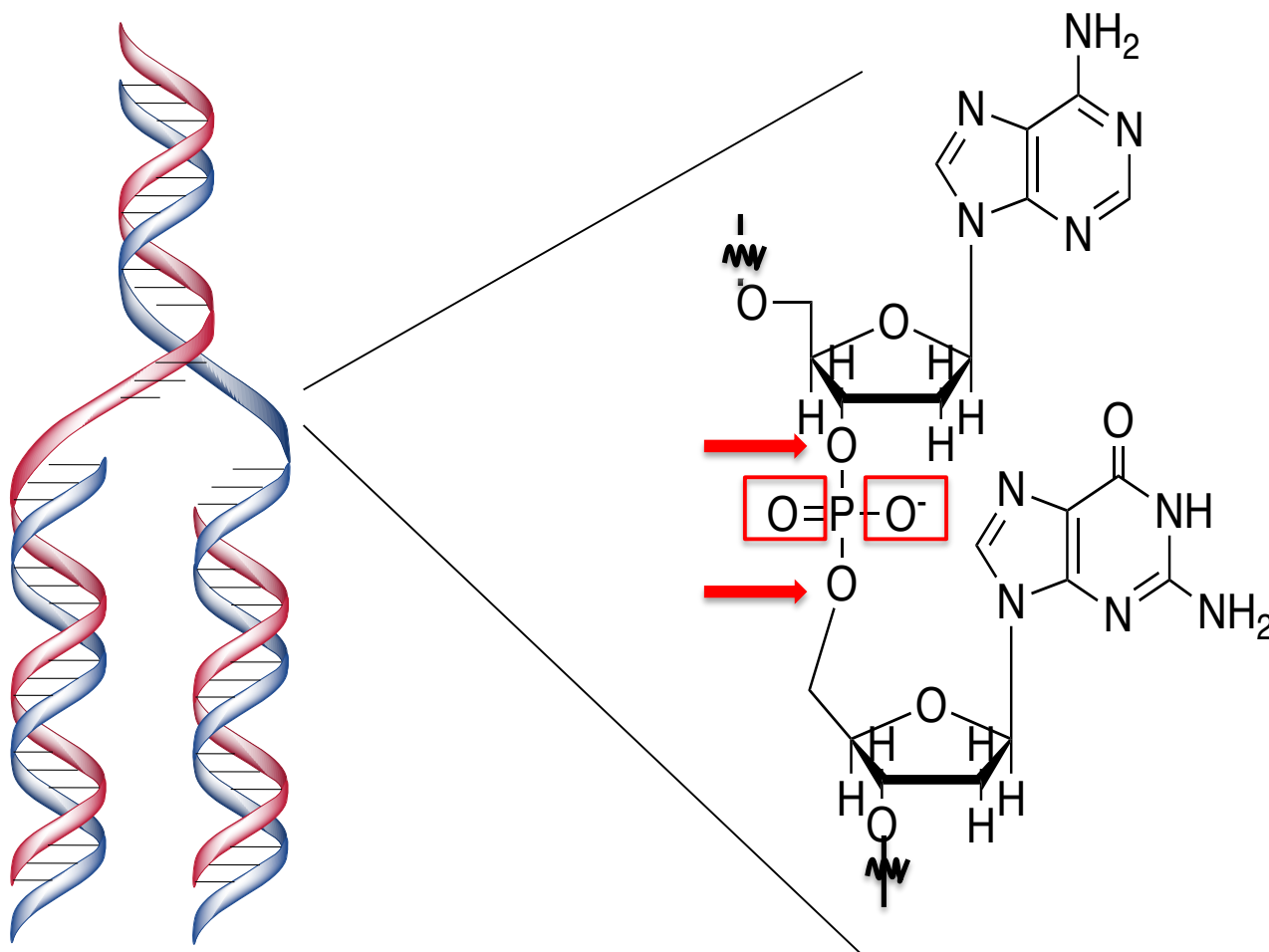


Figure 7. Magnified Model of DNA Showing Phosphodiester Linkage. The red arrows point to the two bridging oxygen atoms connecting the bases. For the bond creation, a nucleotide provides the 3' hydroxyl to attack the phosphorus of the other nucleotide. The non-bridging oxygen atoms are labeled with red boxes.

co-activator to the lac operon to initiate transcription within *E. coli* (Pastan and Perlman 1970). Secondary messengers and their corresponding enzymes should be studied considering the roles the molecules can play within biology.

Without enzymes, phosphoryl transfers are slow and not favorable in aqueous conditions. For DNA and RNA, their half-lives are 140,000 years and 110 year; respectively (Schroeder et al. 2006, Bonfá et al. 2003). For cAMP the half-life is even longer at 732,000 years (Chin and Zhou 1987). Despite this kinetic stability, they are thermodynamically unstable. Being kinetically stable allows for the signaling molecule to conserve its identity by being less susceptible to nucleophilic attack. Maintaining structure is essential considering that lack of cAMP can lead to diseases, such as eczema. Thus, phosphodiester bond makes cAMP less reactive through its kinetic stability. On the other hand, enzymes are able to take advantage of the thermodynamic instability to catalyze the hydrolysis of phosphodiester. This is due to the fact that the products are lower in energy than the reactants leading to an exothermic reaction. Thus, this combination allows for control over signaling through PDE catalysis, which can be through the use of metal ions.

Metal Ion Catalysis

Metal ions are significant in enzyme catalysis because metal ions stabilize negative charges promoting the reaction in three distinct ways: stabilization of the electrophile, activation of the nucleophile, or stabilization of the leaving group (Figure 8) (Christian et al. 2010). When metal ions are active in electrophilic catalysis (Figure 8A), they can stabilize the electronegative atom to pull the electron density in one direction

(Fersht 1999). This allows for nucleophiles to come in and attack the molecule at a more electrophilic site. Electrophilic stabilization pulls electron density away from the phosphorus atom through the coordination with the non-bridging oxygen atoms (Figure 8A). The larger dipole increases likelihood of nucleophilic attack due to decreased electrostatic repulsion. The metal ion can also activate the nucleophile, in an environment of neutral pH, by coordinating with a water molecule and activating it as a nucleophile for attack at the phosphorus atom (Figure 8B). The metal ion complexes can deprotonate water, which creates a metal-hydroxide, a stronger nucleophile compared to water. Any increase in electron density on the nucleophile can cause a rate enhancement on the reaction (Anderson 2006). Along with promoting deprotonation, the metal-hydroxide will foster spatial pre-organization of the nucleophile to position for attack. When the metal ion coordinates to the 3' oxygen, stabilization of the developing negative charge on leaving group allows for the reaction rate to increase (Figure 8C). When the positively charged metal ions interact with the negative charge of the leaving groups, the stabilization increases leaving group bond breaking rate. PDEs can use these mechanisms to stabilize the activation energy and shorten the half-life of cAMP.

Model Systems

Model systems can allow for the study of mechanisms by which enzymes catalyze reactions by simplifying the experiment to focus on one variable. Model systems have been used since 1820 to identify the catalytic role of metal ions (Lehninger 1950). DNA and RNA models have been developed to understand the cleavage of the phosphodiester bonds through metal ions. When comparing hydrolysis between DNA and RNA, there are

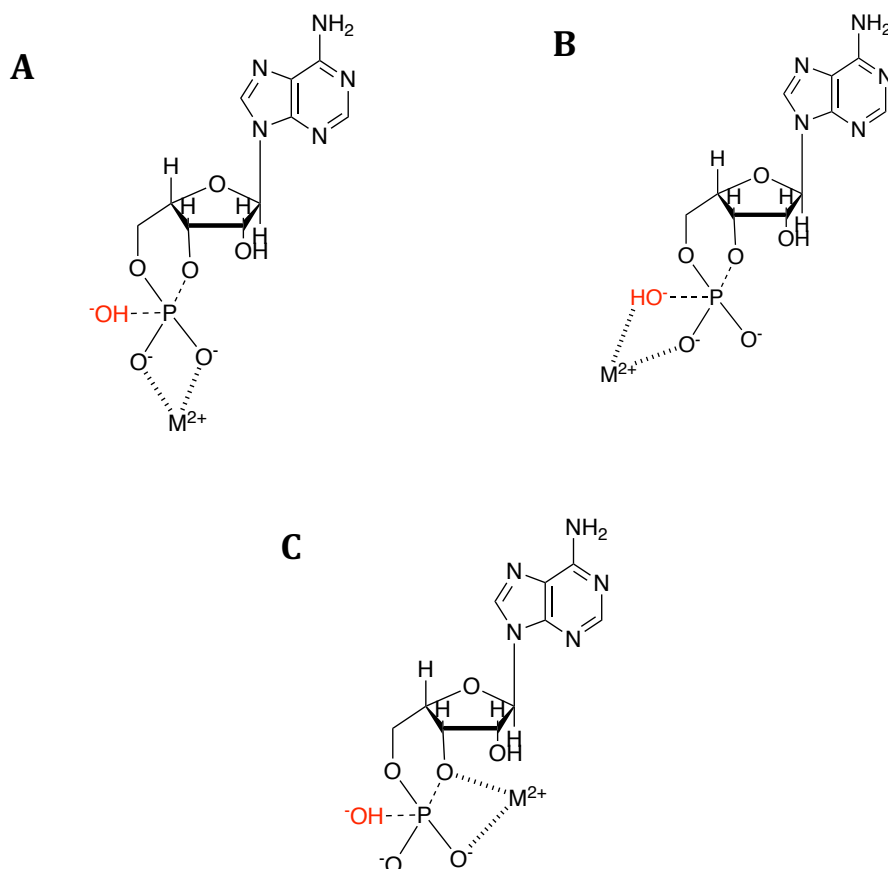


Figure 8. Metal Ion Catalysis Methods of cAMP

Dashed lines between nucleophile and leaving group show breakage or formation of a covalent bond. Nucleophile is labeled in red. Dotted lines show non-covalent interactions between metals coordinating with oxygen atoms. **A.** Electrophilic catalysis shown by the coordination of the metal ion to the two non-bridging oxygens to reduce electrostatic repulsion. **B.** Nucleophilic activation shown by the coordination of the metal-hydroxide. **C.** Leaving group stabilization shown by the metal ion coordinating with the 3' oxygen.

distinctive features (Figure 9). The first is that there is an internal nucleophile for RNA while DNA requires an external nucleophile. RNA has the internal nucleophile provided by the 2' hydroxyl on the base which can be activated and then allow for attack of the phosphodiester. DNA does not have a 2' hydroxyl, thus requiring an external hydroxyl as a nucleophile.

Model systems have been developed to study both RNA and DNA models. In 1996 the study of lanthanides, specifically La (III) ions, with the RNA model, ApA, the researchers found that the metal ions dimerize to create a 13 second half-life for ApA by metal ion catalysis (Hurst et al. 1996). Through HPLC analysis and kinetic assays at different pH levels, a pseudo-first-order rate constant was found. This supported the dimerization conclusion. In comparison, DNA model studies with lanthanides and bis(nitrophenyl) phosphate has shown that the rate of catalysis (k_{cat}) with the lanthanides between La^{3+} and Er^{3+} are approximately 66 times higher (Roigk et al. 1997). The metal ions giving on average a 10-100 higher fold in cleavage based on the lanthanide. A study was published in 1998 on phosphoromonothioate analogues of 3',5'-Up(s)U, another RNA model, with Zn^{2+} , Cd^{2+} , Gd^{3+} , Mn^{2+} , and Mg^{2+} (Ora et al. 1998). Using phosphoromonothioates allowed for the investigation of where the metal ion coordinated and interpretation of the stereochemistry by comparing the kinetics. The results were used for comparison to analyze catalytic abilities and the mechanism of cleavage. Researchers saw first order for the metal ion catalyzed and NaOH reactions. Zn^{2+} , Cd^{2+} , and Gd^{3+} catalyzed reactions were relatively faster than those of Mn^{2+} and Mg^{2+} .

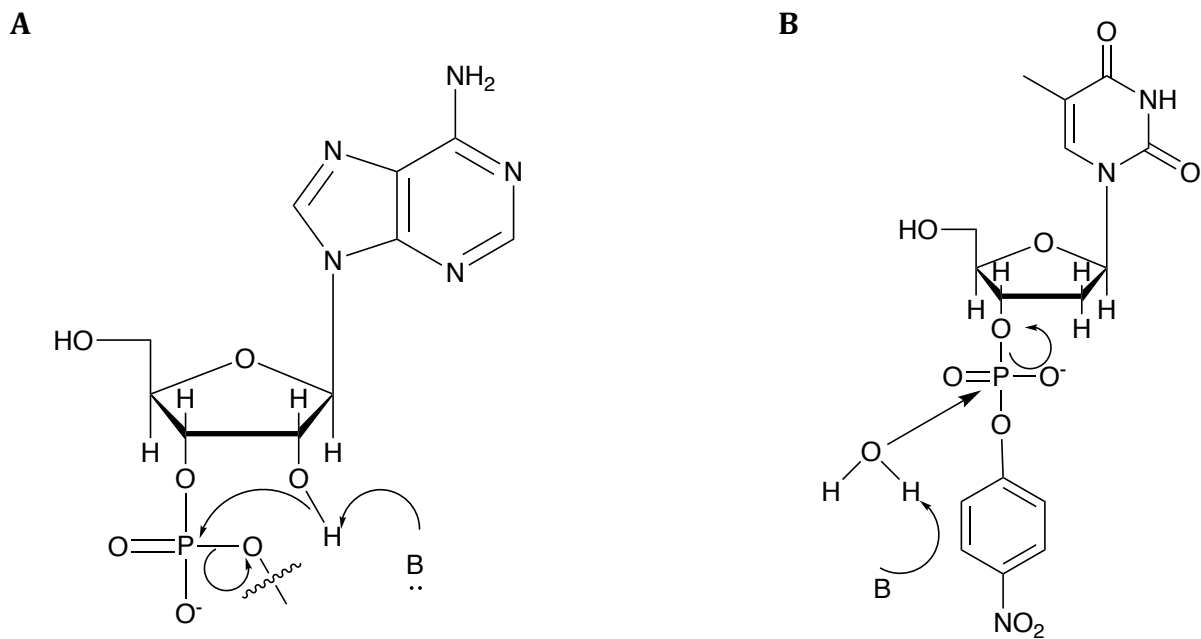


Figure 9. RNA versus DNA Model Hydrolysis

B is showing a general base activation of water **A**. RNA hydrolysis shows an internal nucleophile with a poor alkyl ester leaving group. **B**. DNA model T5PNP hydrolysis shows an activated external nucleophile attacking and a good leaving group.

Mechanistically, it was determined that there is an "in-line mechanism" where the phosphorus is inverted and does not undergo pseudo-rotation. Studies on uridine 3'-alkyl phosphates and 3'-aryl phosphates, RNA models, with Zn^{2+} have shown metal ion capabilities in catalyzing through leaving group stabilization (Mikkola et al. 1999). This was seen through the higher rate enhancement as the leaving group became worse, showing general acid catalysis. Further studies done on uridine 3'-phosphodiester showed that metal ions could act through general base or acid catalysis depending on the leaving group and the acidity of the metal ion (Korhonen et al. 2013). These different model systems were able to record the rates that metal ions provide in catalysis, and therefore elucidate mechanisms.

When developing a model system, it is important to compare to the other systems to note similarities or differences. Within the model systems developed in the Cassano laboratory at Drew University, examination of metal dependence of these mechanisms for DNA and RNA hydrolysis in aqueous solution reveals a difference in the number of metal ions. DNA has two metal ions coordinating for catalysis while RNA has one (Kirk et al. 2009, Messina 2013). The thymidine-5'-*p*-nitrophenyl phosphate model system has been useful as a DNA model system (Kirk et al. 2009). Studies done with magnesium and calcium gave insight to the mechanisms by which catalysis occurs. Calcium in particular showed to have a multinuclear mechanism through analysis of rate constants. The Cassano laboratory has developed an RNA model with UpG, a RNA dinucleotide, which favors a one metal ion mechanism. The mechanism was found using primary and secondary kinetic plots with this model (Messina 2013). Primary plots involve graphing

the mole percentage of each product and reactant over the course of time. This allows for calculations of rate constants, which can be graphed against their respective calcium concentration to analyze the secondary plots. Based on the type of curve that is fit to these data sets, the mechanism of catalysis can be differentiated (Figure 10).

Analysis of the graphs showed a multi nuclear mechanism for DNA and a single ion mechanism for RNA. The DNA model system fits best to a quadratic fit, correlating that type with a multinuclear mechanism (Figure 10A). The RNA model system fits a rectangular hyperbola, correlating with a single nuclear mechanism with binding of the metal prior to the reaction (Figure 10B). When comparing the RNA model system to the DNA model system, there are two major types of cleavage that are covered. The RNA model system portrays the cleavage of a molecule with an internal nucleophile and a poor leaving group. The DNA model system analyzes the cleavage of a molecule with an external nucleophile and a good leaving group. It is unclear whether number of the Ca^{2+} involved in catalysis is related to leaving group stability or the type of nucleophile. A model system with cAMP can investigate this questions since the molecule has an external nucleophile and poor leaving group, as shown by the crystal structure, thus creating a new way to study such molecules. Model systems for cAMP have also been explored.

Exploring current model systems within literature for cAMP showed little information on kinetics of metal ion catalysis. The first model system for cAMP was with barium hydroxide complex, $\text{Ba}(\text{OH})_2$, and cAMP resulting in 3'AMP and 5'AMP (Mehdi et al. 1982). There was a ratio of 4:1 of 3'AMP to 5'AMP in products. Analysis

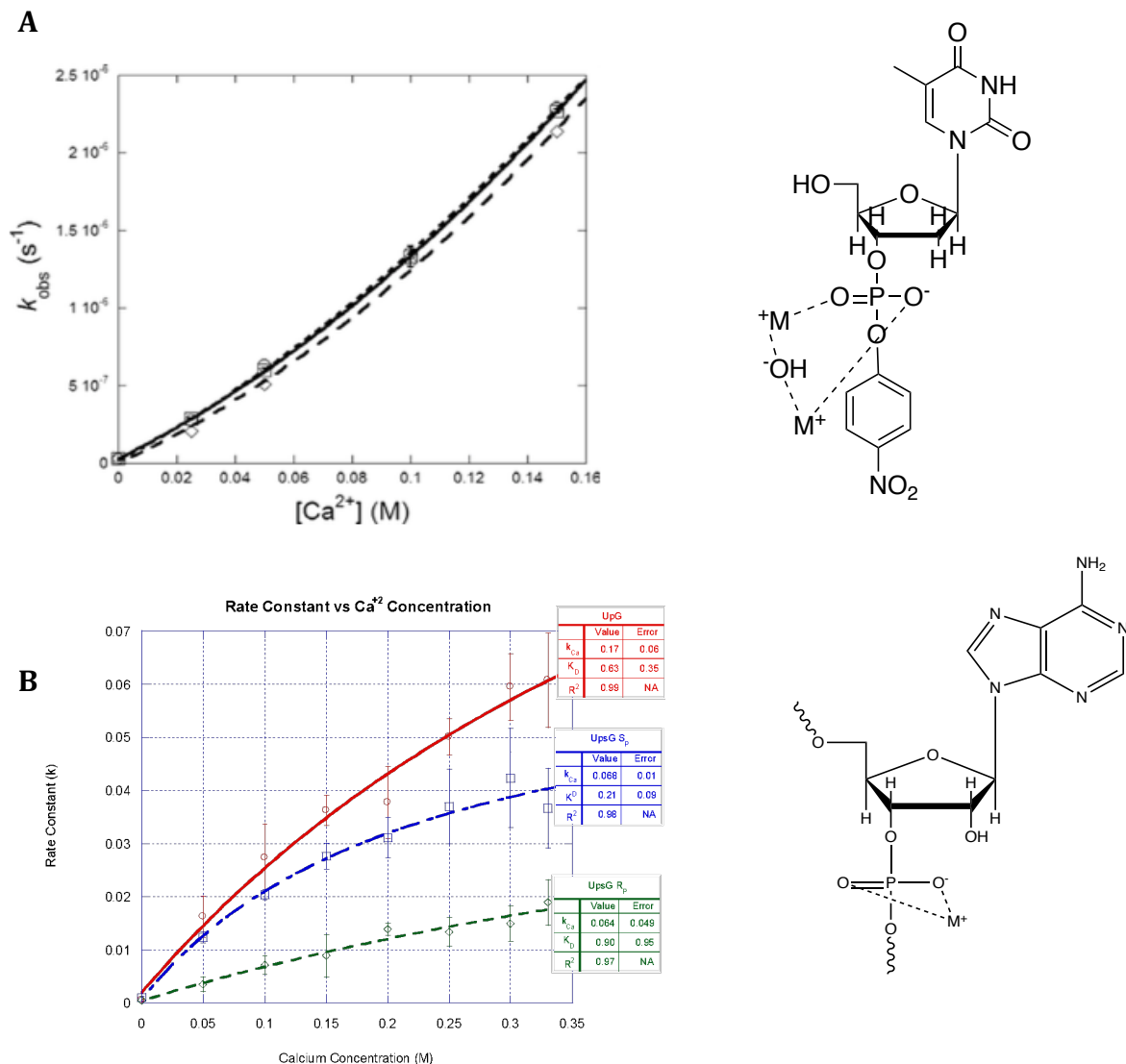


Figure 10. Secondary Plots to Differentiate Metal Ion Mechanisms

A. Secondary plot of rate, k_{obs} , versus calcium concentration for the DNA model, T5PNP, shows a quadratic fit. This correlates with DNA phosphodiester model, T5PNP, with two metal ions coordinating for a binuclear mechanism **B.** Secondary plot of rate versus calcium concentration for the RNA model shows a downward exponential curve for UpG and the UpG thioates. Thus, RNA phosphodiester with one metal ion coordinating for a mononuclear mechanism (Adapted from Kirk et al. 2008, Messina 2013)

of stereochemistry showed that there was attack at phosphorus and inversion, thus pseudorotation was unnecessary. However, the catalytic metal ion effect was not investigated. Another model system for cAMP was conducted using cobalt (trien) metal ions (Chin and Zhou 1987). However, this only allowed for the analysis of the production of adenosine as opposed to 3'AMP and 5'AMP (Figure 11). There is intense electrophilic catalysis of the phosphoryl transfer causing approximately a 10^8 fold in catalysis (Chin and Zhou 1987). When the cobalt coordinates, with the non-bridging oxygen atoms, the stabilization of the negative charges allows for the nucleophilic attack to proceed much more quickly.

Current model systems do not serve for good comparison between the DNA and RNA model system. The hydrolysis of the intermediates, 3'AMP and 5'AMP, happened faster than the hydrolysis of cAMP. Thus, the intermediates were not observed making it unclear if 3'AMP, 5'AMP, or both were produced. The high catalytic abilities of cobalt prevented the model system from showing 3'AMP and 5'AMP as products. Similar results were observed when cAMP was cleaved with high concentrations of sodium hydroxide with no divalent metals present. Due to the limitation of this model system, it is important to find another to further the analysis of metal ion assisted hydrolysis of cAMP.

Current Work

The model system that we are developed is one to study the metal ion catalysis using cAMP and Ca^{2+} . Ca^{2+} was chosen since it is in the same group as magnesium, a frequently used metal ion within physiological systems. Magnesium could not be used within this model system because it will precipitate out at the high pH levels necessary to achieve reasonable rates of reaction. Analysis of the model system was through kinetic

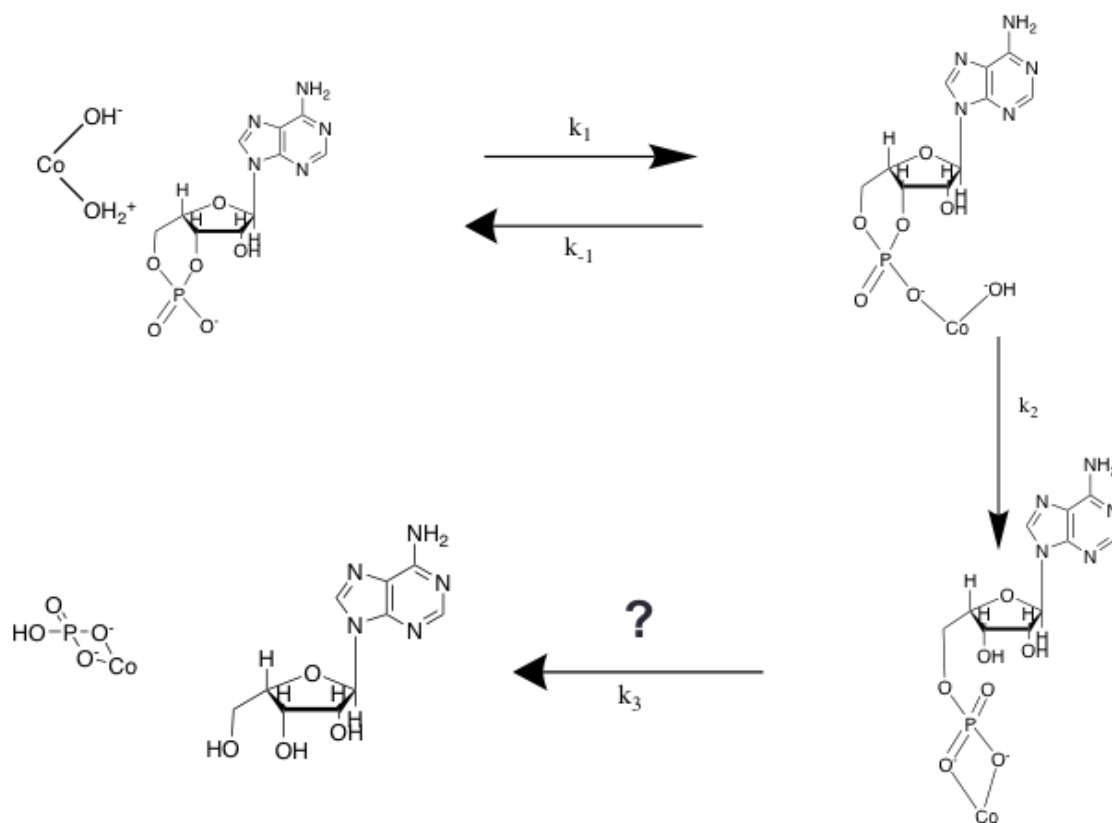


Figure 11. Cobalt Metal Ion Model System Reaction Scheme. The cAMP and cobalt metal ion model system yielded the products adenosine and phosphate. The scheme starts with the cobalt coordinated to water, hydroxide, and cAMP. The cobalt coordinated the hydroxide for attack, and the non-bridging oxygens for electrophilic catalysis. Finally, the products adenosine and phosphate can be seen, and the rate constants of 3' and 5' AMP could not be collected since these products cannot be isolated (Adapted from Chin and Zhou 1987).

assays, isotope reactions, mass spectroscopy and HPLC. The data provided by the model systems was analyzed by calculating kinetic constants and investigating how they differ based on the Ca^{2+} concentrations that were manipulated. Throughout the research on cAMP, the products with the model system were determined to be 3'AMP and 5'AMP. There was differing ratio of these products based on calcium concentration, where there was a higher production of 3'AMP versus 5'AMP in the presence of increasing amounts of Ca^{2+} . Thus, one of the questions we addressed in our research is why we are seeing such a ratio along with how many metal ions are coordination; also, what is the mechanism by which hydrolysis occurs.

Mechanisms based on aqueous model systems of phosphodiester hydrolysis show that 99% of the hydroxyl attack happens at the carbon versus the phosphorus (Figure 12) (Schroeder 2006). This can be attributed to the negative charge that is surrounding the phosphorus while the carbon does not have a charge to repel the attack. Carbon is thus more susceptible to nucleophilic attack in aqueous solution versus phosphorus. However, the mechanism for hydrolysis by PDEs always involves attack at the phosphorus atom (Huai et al. 2003). This is due to the facilitation by the enzyme and the environment that is made within the active site. Thus, another question that we investigated was where the hydroxide attack occurs with the metal ion facilitation.

To do so, we used isotope-substituted ^{18}O water for our reactions (Figure 13). This incorporated the isotope into the 5'AMP and 3'AMP products, as confirmed using mass spectroscopy. These products were hydrolyzed by alkaline phosphatase to remove the phosphate group, so that just the adenosine could be isolated through HPLC. Analysis

with mass spectroscopy allowed visualization of whether the ^{18}O was incorporated into the phosphate group or the adenosine. Knowing the place of nucleophilic attack may help in understanding the ratio of products.

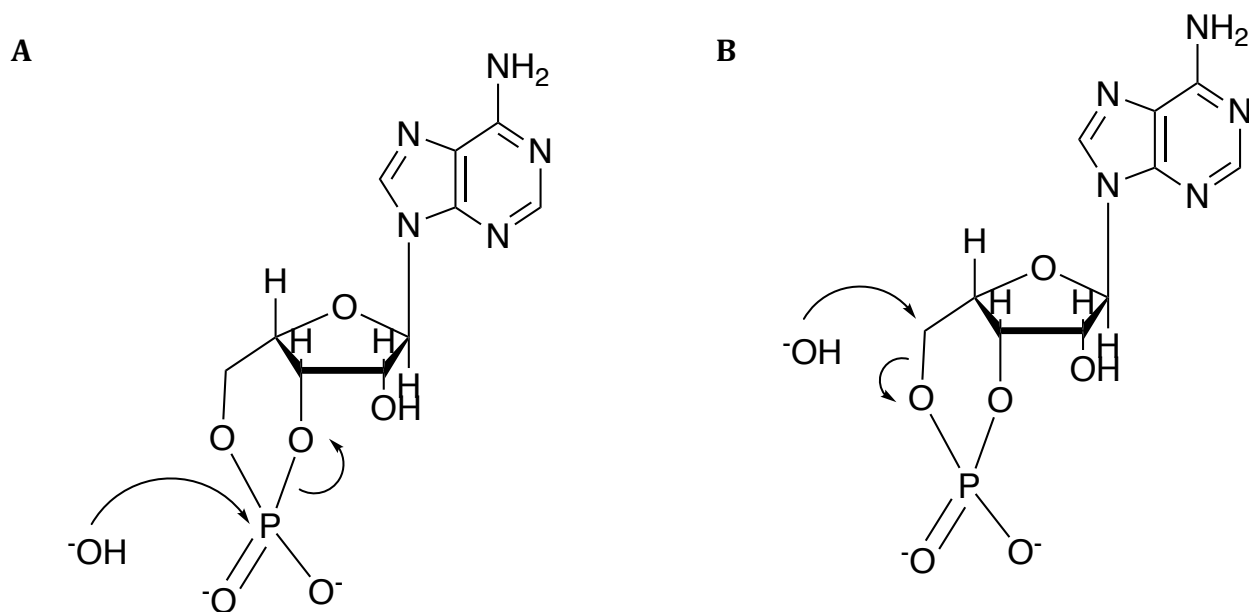


Figure 12. Attack at Phosphorus Versus Carbon

A. Attack at phosphorus by hydroxide. **B.** Attack at carbon by hydroxide which eventually leads to the production of 3'AMP.

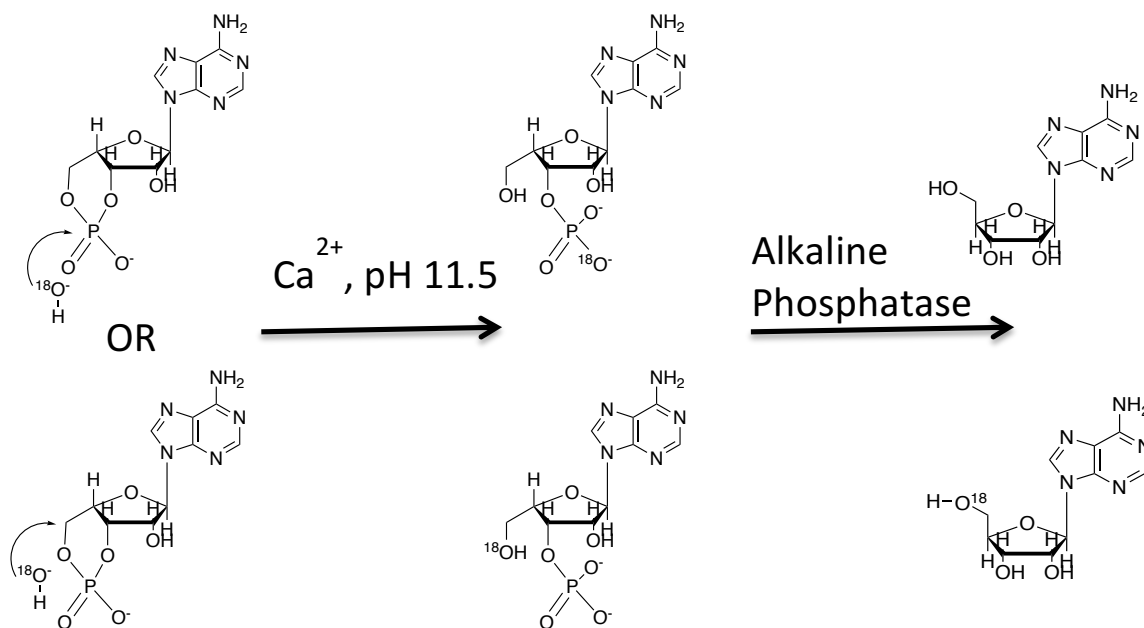


Figure 13. Isotope Assay Reaction Scheme. The top scheme shows attack at the phosphorus atom while the bottom scheme shows attack at the carbon. Both schemes show 5'AMP as the intermediates formed (3'AMP not shown). The cAMP was initially incubated with ^{18}O water to allow for incorporation into the 3'AMP and 5'AMP. Then 3'AMP and 5'AMP were treated with alkaline phosphatase, which specifically removes the phosphate. Afterwards, the products were checked for heavy isotope incorporation to understand whether the initial attack happened at the carbon or phosphorus atom.

Methods

Kinetic Assays

Sample Preparation

Reactions were conducted at 48 °C at pH 11.5 maintained by 50 mM N-cyclohexyl-3-aminopropanesulfonic acid (CAPS). The reactions included 100 μM of cAMP, 50 mM CAPS, variable concentrations (0-0.33 M) of CaCl₂, and H₂O to a total volume of 500 μL. To retain an ionic strength of 1.0, each solution had additional NaCl. At different time points, 50 μL aliquots were taken from the reaction and neutralized with 60 μL 87.5 mM 4-(2-hydroxyethyl)-1-piperazinepropanesulfonic acid (EPPS free acid) to approximately a pH of 7. A control reaction without cAMP for the unknown peak was conducted by using a reaction mixture of water, 0.33M CaCl₂, and 50 mM CAPS buffer at pH 11.5 in a total volume of 500 μL. At different time points, 50 μL aliquots were taken from the reaction and neutralized with 60 μL 87.5 mM EPPS free acid to approximately a pH of 7-8. The samples were frozen at -20 °C until they could further be analyzed by HPLC.

The NaOH reactions were conducted in the same manner as the previous reaction but 1 M NaOH substituted CAPS and CaCl₂. At different time points, 50 μL aliquots were taken from the reaction and neutralized with 60 μL 87.5 mM EPPS free acid and HCl (50/50 mixture) to a pH of approximately 7. The samples were frozen at -20 °C until they could further be analyzed through HPLC.

High Pressure Liquid Chromatography

Reactions were analyzed through Agilent 1100 Series HPLC. The stationary phase was a non-polar C18 column, ZORBAX 300 SCB 4.6mmX15cm. The mobile phase consisted of a gradient of 0.1 M ammonium acetate/2% acetonitrile for twenty minutes, and a mixture of 95% acetonitrile and 5% water was increased from 0% to 20% for the remaining five minutes of the run at twenty minutes to decrease the polarity. Peaks were associated with compounds based on their retention time and peak shape. Peak area was integrated, and mole fractions were graphed and fit using Kaleidagraph™. Peaks were identified by mass spectrometry and in comparison with standards.

Mass Spectroscopy

A Waters Micromass LCT Premier mass spectrometer (MS) utilizes electron spray ionization and time-of-flight (ESI-TOF) method under positive ion mode. Peaks collected through the HPLC were injected through direction infusion at 10 μ L/minute. The samples were analyzed for the expected product masses of cAMP (331 m/z), 5'AMP/3'AMP (349 m/z), and adenosine (268 m/z). The ESI conditions included a capillary of 3.2 kV, cone voltage of 35 V, desolvation temperature of 220 °C, source temperature of 90 °C, gas flow of 800 L/hr.

Kinetic Analysis using Kaleidagraph™

The mole percentage was graphed against the change in time for the primary plot. Cyclic AMP was fit with an exponential decay equation (Equation 1) while the products, 5'AMP and 3'AMP, were fit with a quadratic growth equation (Equation 2) to analyze the primary plot.

$$\text{Exponential Decay: } A_t = A_0 * e^{-kt} \quad \text{(Equation 1)}$$

$$\text{Quadratic growth: } A_t = B - A_0 * e^{-kt} \quad \text{(Equation 2)}$$

A_0 is the initial concentration of molecule and A_t is the concentration of that same molecule at time (t). The k represents the first order rate constant and t represents time. The B in Equation 2 represents the expected maximum of the product. The ratios of the products, 3'AMP and 5'AMP, were graphed against the concentrations of calcium. Ratios for the lower concentrations, 0.05 M-0.15 M, were calculated through Kaleidagraph™ by inputting the rate constant from cAMP decay. The rate constants were graphed against the concentrations of calcium and fit with a quadratic formula for the secondary plot (Equation 3).

$$\text{Quadratic Formula: } k_{\text{obs}} = k_0 + k_{1\text{st}} [\text{Ca}^{2+}] + k_{2\text{nd}} [\text{Ca}^{2+}]^2 \quad \text{(Equation 3)}$$

Isotope Assays

Sample Preparation

Reactions were conducted at 48 °C at pH 11.5 maintained by 50 mM CAPS. The reactions included 4 mM of cAMP, ^{18}O H₂O (or ^{16}O H₂O for the controls), 0.5 M CAPS, and 0.33 M concentration of CaCl₂, with a total volume of 500 μL. Samples were incubated at 48 °C for 168 hours before neutralization with EPPS free acid. The products, 3'AMP and 5'AMP, were separated and collected through the HPLC. Samples were lyophilized and re-suspended in Millipore water to measure ultraviolet (UV) absorbance approximately 2-3 times. Concentrations of the samples were calculated using absorbance, Beer's Law, and extinction coefficient. The products were analyzed using TOF MS to determine whether the ^{18}O was incorporated into the products.

Shrimp alkaline phosphatase (SAP) reactions were set up with 3'AMP and 5'AMP products containing ^{18}O . Recombinant SAP (rSAP) was purchased from New England BioLabs and stored at $-20\text{ }^{\circ}\text{C}$. Reactions with 1 pmol of 3'AMP or 5'AMP, CutSmart Buffer (10X), 1 unit of rSAP, and H_2O were prepared to a total volume of 20 μL . The reactions were heated for 30 minutes at $37\text{ }^{\circ}\text{C}$. Alkaline phosphatase was inactivated for 5 minutes at $65\text{ }^{\circ}\text{C}$. The samples were frozen at $-20\text{ }^{\circ}\text{C}$. The adenosine peaks were collected by HPLC for the 3'AMP and 5'AMP alkaline phosphatase assays.

Mass Spectroscopy for Isotope Analysis

A Waters Micromass LCT Premier MS utilizes electrospray quadrupole mass spectrometry method under positive ion mode. Peaks collected through the HPLC were injected through direction infusion at 10 $\mu\text{L}/\text{minute}$. Each respective adenosine peak was dried down and re-suspended in 50/50/0.1% of water/acetonitrile/acetic acid for mass spectroscopy analysis. Masses were analyzed to determine when the ^{18}O was incorporated or removed. The conditions included a capillary of 3.2 kV, cone voltage of 35 V, desolvation temperature of $220\text{ }^{\circ}\text{C}$, source temperature of $90\text{ }^{\circ}\text{C}$, gas flow of 800 L/hr.

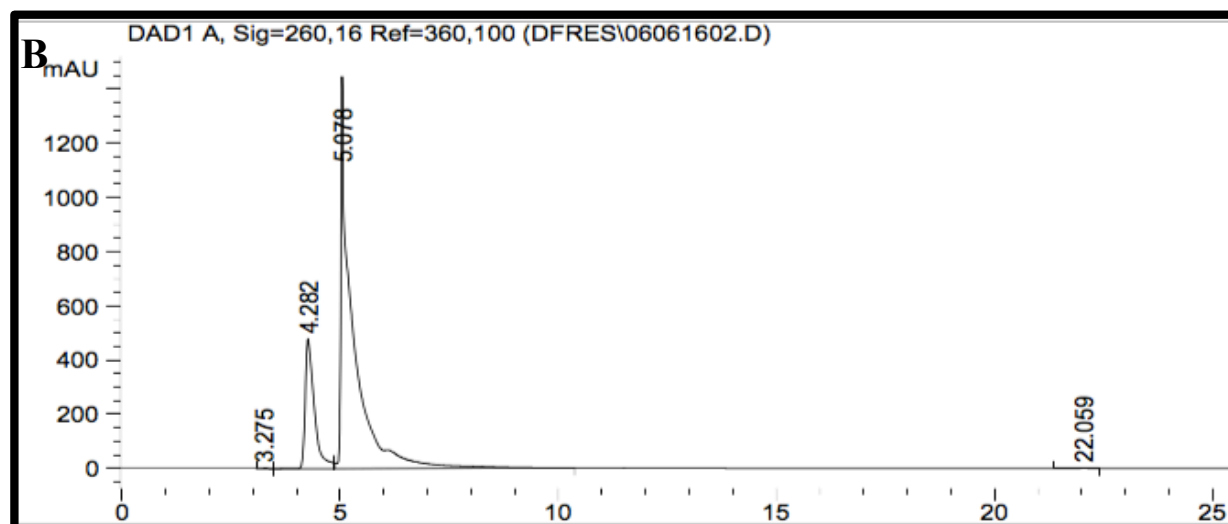
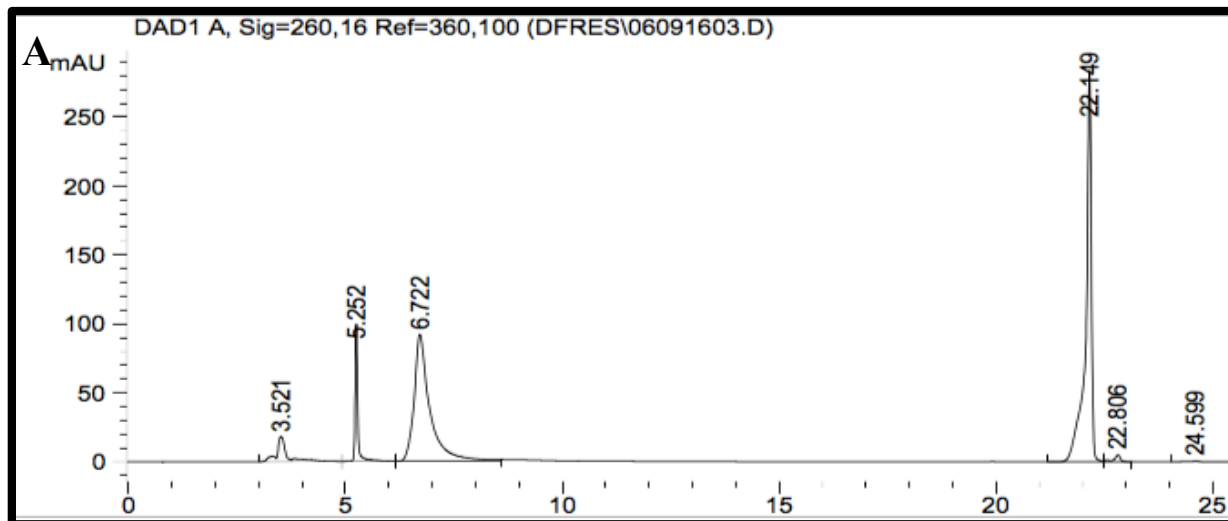
Results

Product and Reactant Identification

Kinetic assays were run with the calcium model system at varying calcium concentrations. HPLC was used to separate out the different molecules within our model system. The elution times and integrations of the peaks correlating with the products and reactant differed on the chromatograph (Figure 14A). Peaks for the products and

reactants were determined using standards run on the HPLC; the shape of the standards peaks and elution times were used as guides to correlate the peaks from reactions. The 5'AMP standard (Figure 14B) shows elution time at approximately five minutes and the chromatograph also shows void volume at approximately 3.5 minutes. The reaction chromatograph (Figure 14A) from a 0.33 M calcium reaction at 33 hours shows a peak at 5.3 minutes consistent with the 5'AMP standard (Figure 14B). The 3'AMP standard (Figure 14C) shows elution time at approximately 7.7 minutes. The reaction chromatograph (Figure 14A) from a 0.33 M calcium reaction at 33 hours shows a peak at 6.7 minutes that correlates with the 3'AMP standard shown (Figure 9B). The cAMP standard (Figure 14D) shows elution time at approximately 21.8 minutes. The reaction chromatograph (Figure 14A) from a 0.33 M calcium reaction at 33 hours shows a peak at 22.1 minutes that correlates with the standard shown in Figure 14D. The peaks from the reaction are also similar in shape to those of the standards showing further correlation. The differences in retention time can be due to human error discrepancies within the making of buffers by which they were run on the HPLC, thus causing a slight shift within the time.

There was also an additional control run for the identification of peaks due to a peak that appeared at approximately 28 minutes on the HPLC chromatograph (Figure 15). The peak did increase over the course of the reaction time. However, when running a control experiment without the addition of cAMP, the peak was still observed growing at the same rate over time. Figure 16 shows the comparison of the no cAMP reactions at 0 hours and at 33 hours. Based on the results of the control experiments, the additional



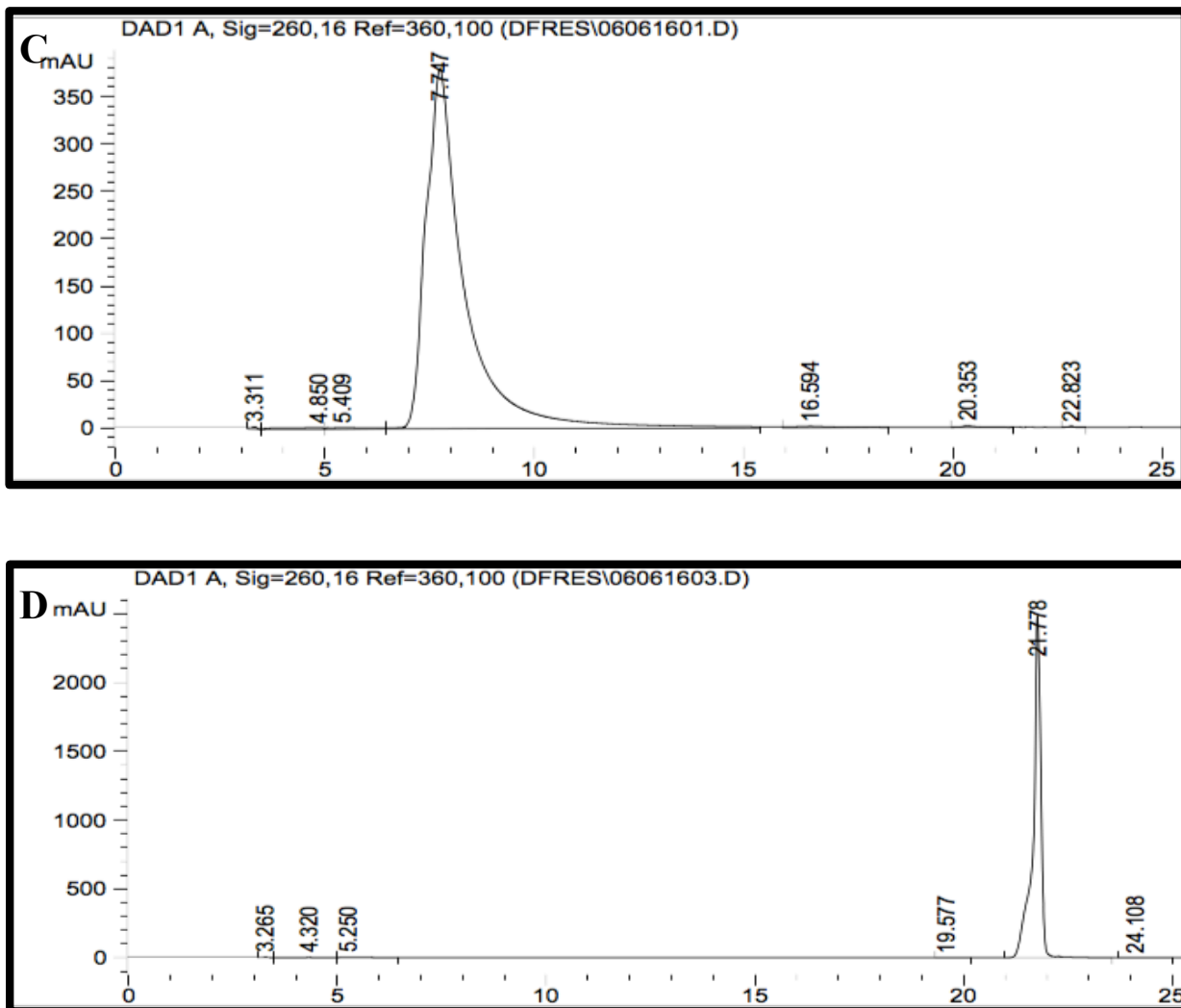


Figure 14. HPLC chromatographs of Standards and Reaction. A. HPLC chromatograph of reaction mixture with 0.33 M calcium and cAMP. **B.** HPLC chromatograph of the 5'AMP standard **C.** HPLC chromatograph of 3'AMP standard **D.** HPLC chromatograph of cAMP standard

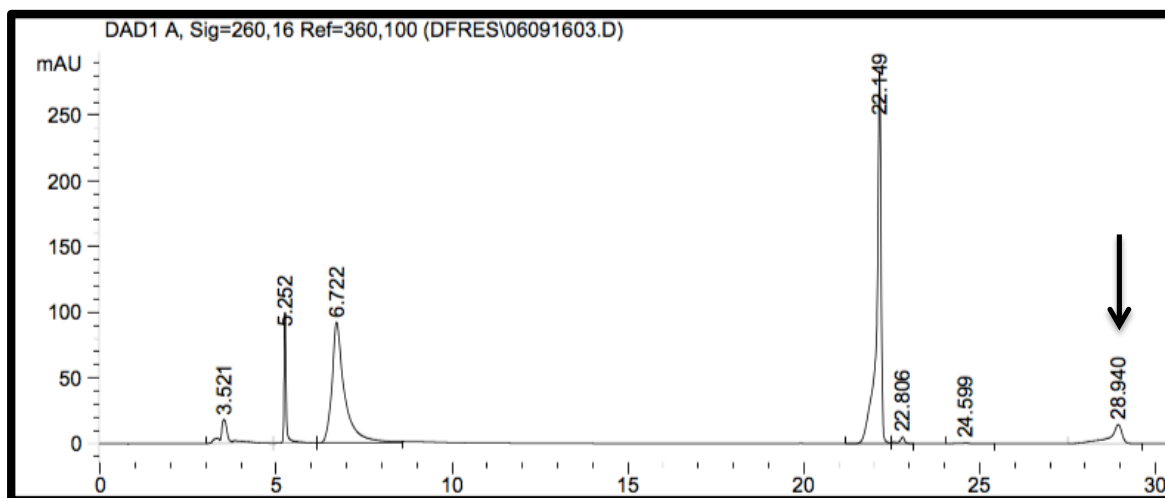


Figure 15. HPLC chromatograph of 0.33 M CaCl₂ Reaction at 33 Hours. At 28.9 minutes there is a minor peak, which was not identified based on standards

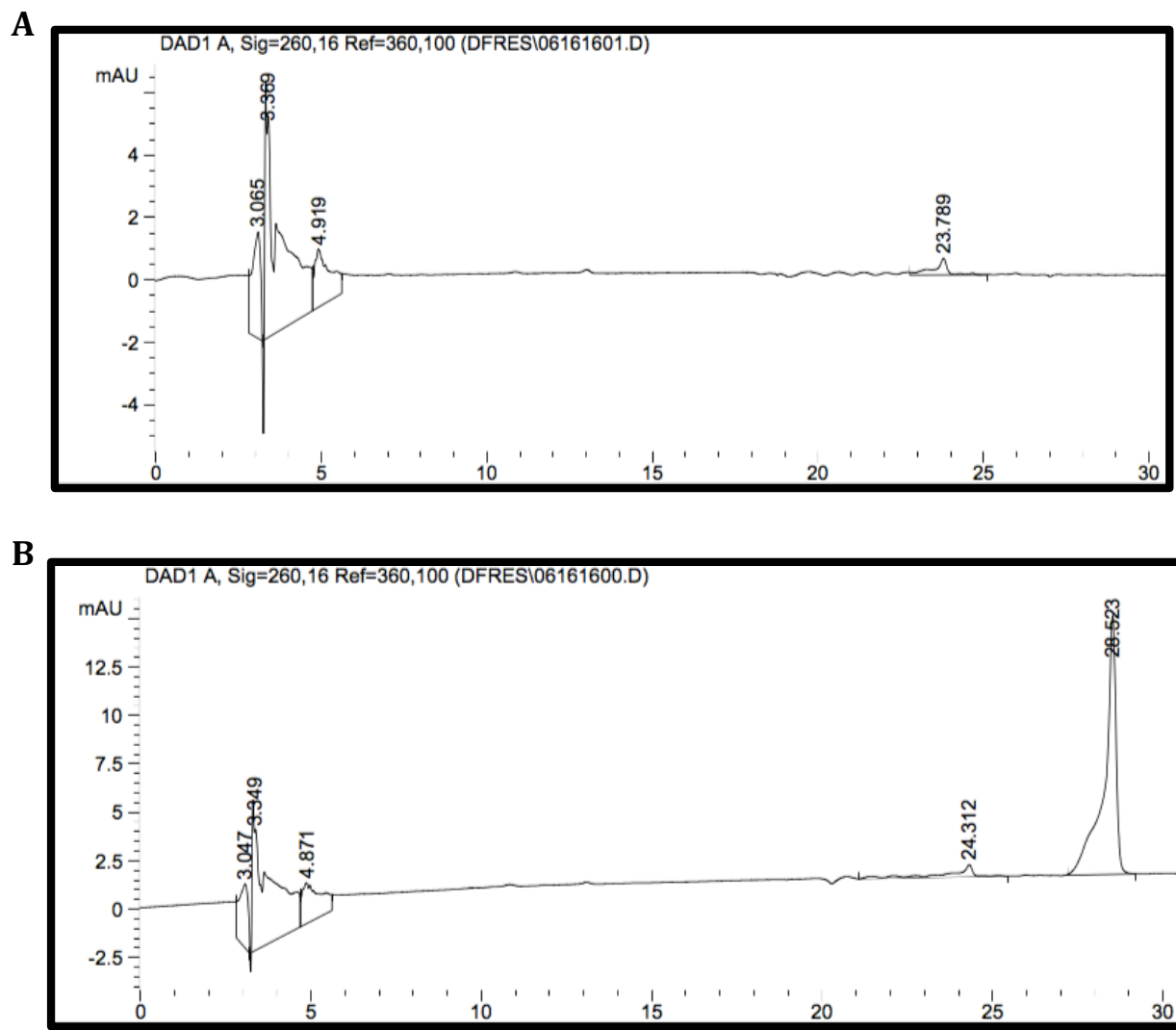


Figure 16. HPLC Chromatographs of Control Experiment

A. HPLC chromatograph of reaction mixture without cAMP at the 0 hour time point. **B.** HPLC chromatograph of reaction mixture without cAMP at the 33 hour time point.

unknown peak is not part of the cAMP and calcium model system.

Furthermore, to analyze products and reactant, overlaying of the chromatographs of reaction mixtures over time showed an increase of the products and decrease of the reactants (Figure 17). The product peaks can be seen at approximately 5 and 6 minutes and the reactant peak at 22 minutes. The 5-minute time point correlates with 5'AMP and the 6-minute time point correlates with 3'AMP. The 22 minute peak is cAMP. There is a clear increase of the product peaks at approximately 5 and 6 minutes while the reactant at 22 minutes decreases over time. The slight differences in retention time can be due to the different buffers by which the reaction mixtures were run. To further validate the identification process, MS was used (Figure 18). The peaks observed were collected through the HPLC, dried, prepped, and ran on the mass spectrometer. The 5 minute peak mass spectrum showed a m/z of 349, consistent with the mass of 5'AMP. The 6 minute peak mass spectrum showed a m/z of 349, consistent with the mass of 3'AMP. The peak at 22 minutes had a mass spectrum that showed a m/z peak of 331, which is consistent with the mass of cAMP. The m/z peaks were consistent with the molecular predictions from the HPLC standards.

Kinetic Analysis

Kinetic analysis gives insight into the metal ion mechanism. To do so, the peaks from the reactions for each product and the cAMP reactant were integrated. The recorded areas for each molecule within the model system were used to calculate the mole percentages. Mole percentages were graphed against time on KaleidagraphTM (Figure 19).

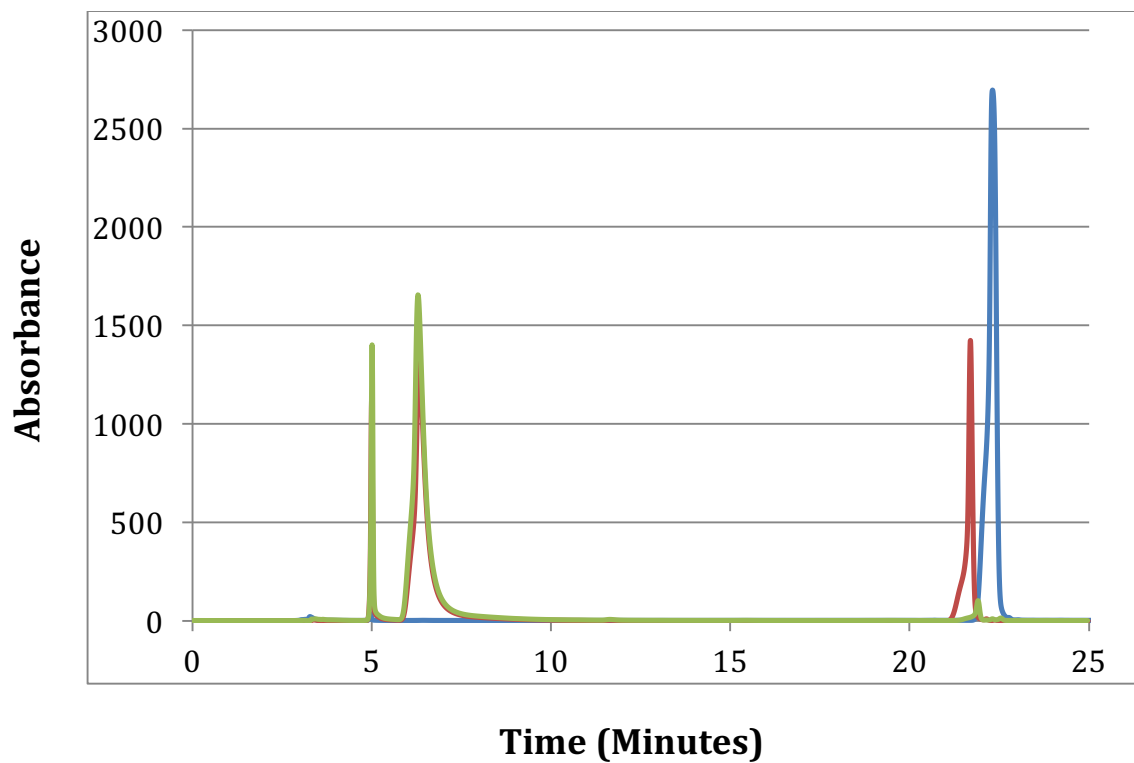
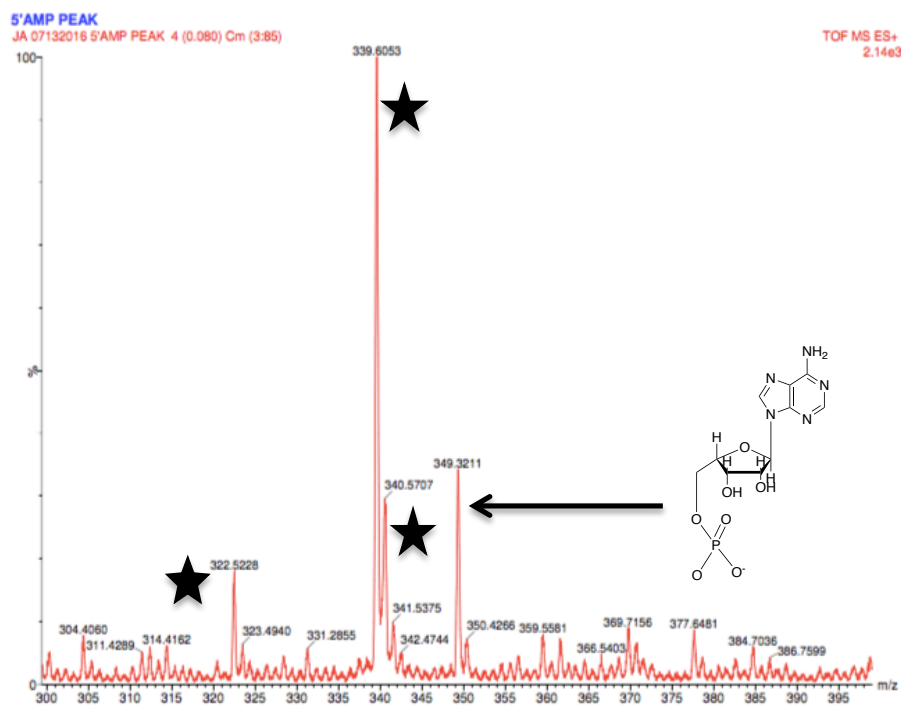
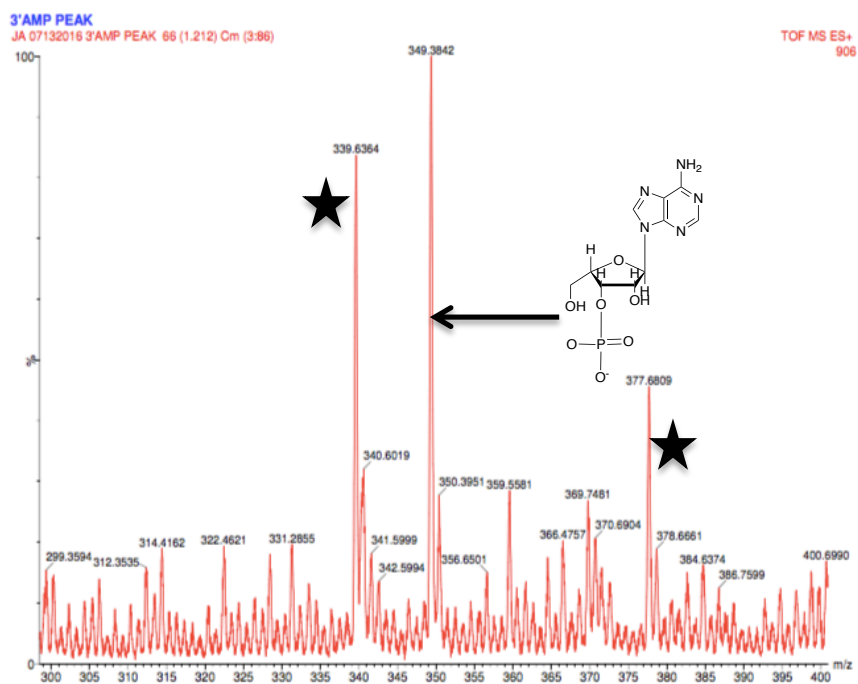


Figure 17. Chromatogram Analysis of 0.33 M CaCl_2 Reaction with cAMP. The 0-hour time point is in blue, 48-hour time point in red, and 168-hour time point in green.

A



B



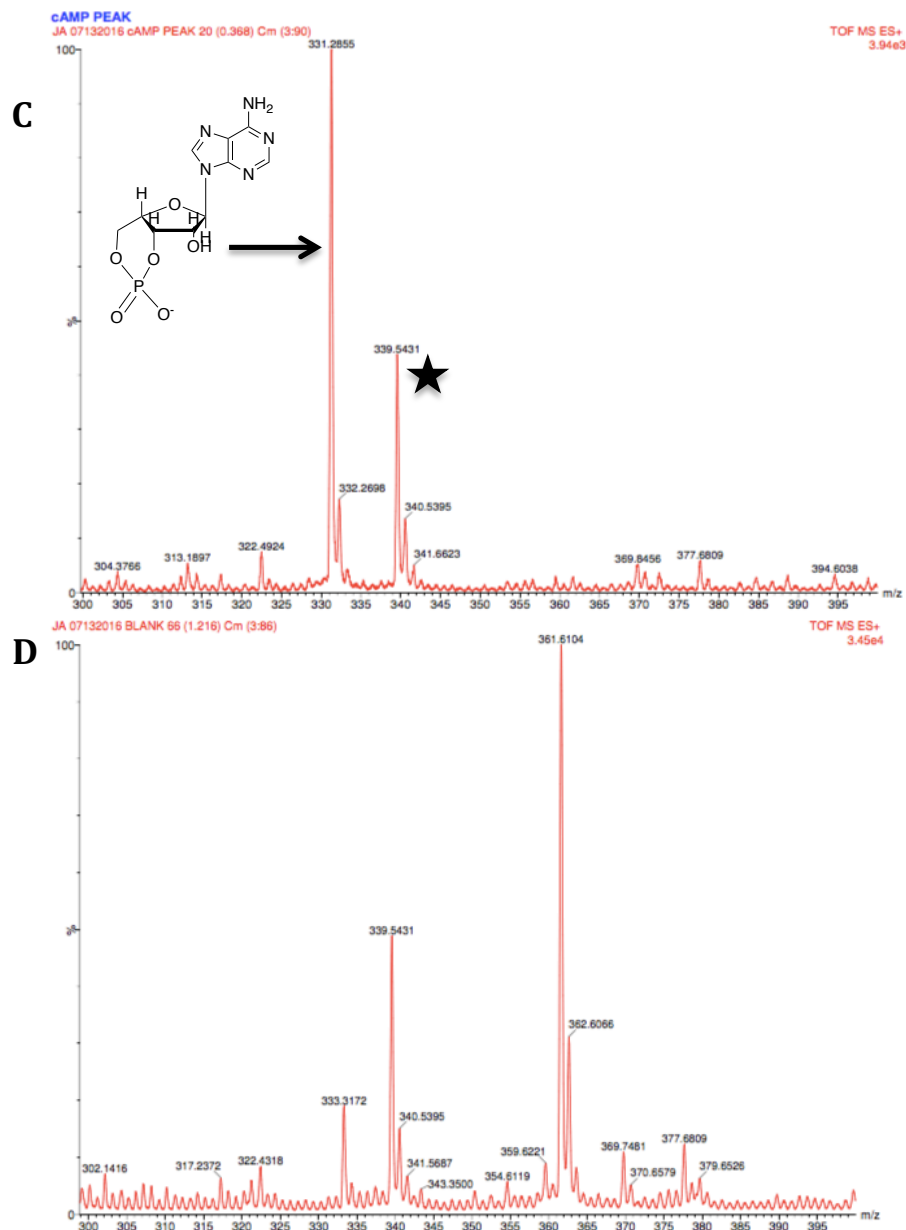


Figure 18. Mass Spectrometry Analysis of 0.33M CaCl₂ Reaction with cAMP using ESI-TOF Method. A-C. Mass Spectra of peaks collected through HPLC analysis. Stars represent the peaks present within the blank **A**. 5-minute peak spectrum which has a 349 m/z peak. **B**. 6-minute peak spectrum which has a 331 m/z peak. **C**. 22-minute peak spectrum which has a 331 m/z peak. **D**. blank consisting of 50% acetonitrile and 50% water. Stars indicate the peaks found within the blank

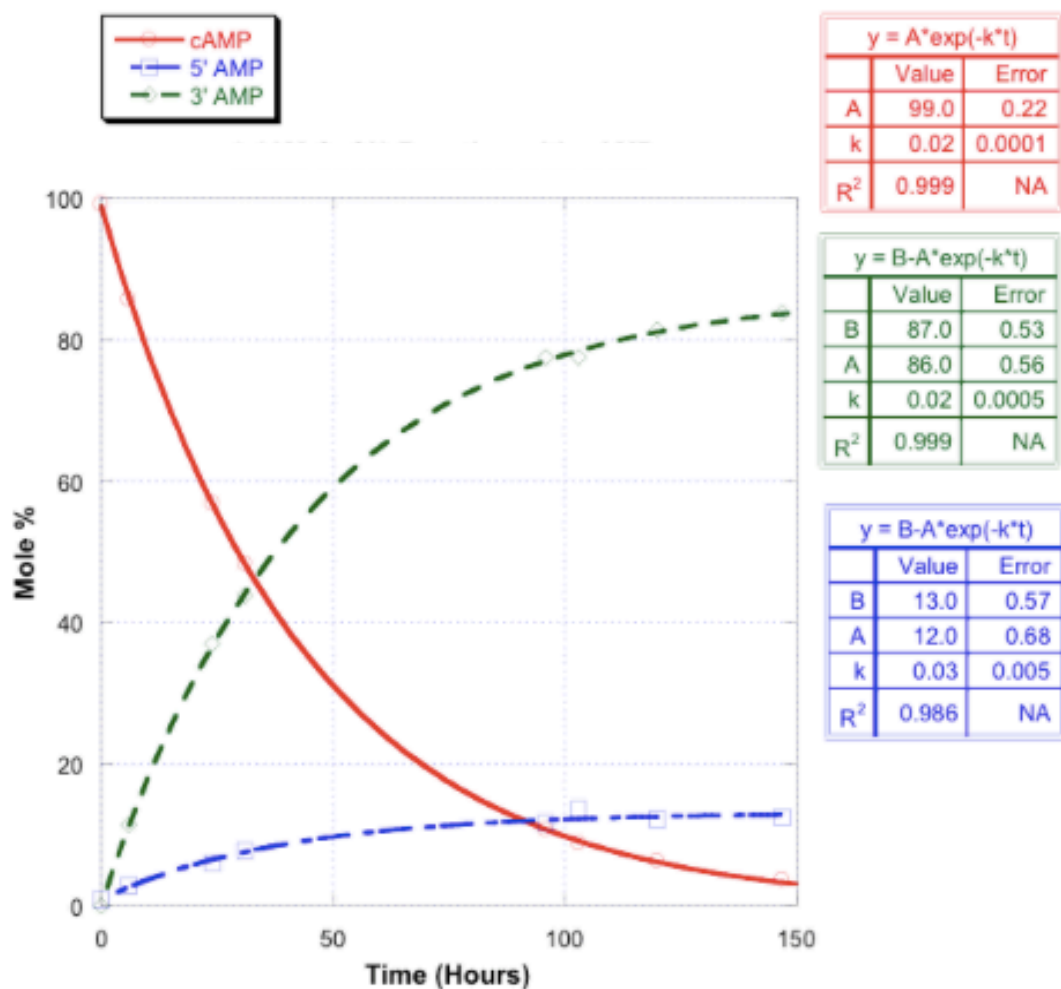


Figure 19. Change in Mole Percentage Over Time for a 0.33 M CaCl₂ Reaction with cAMP. Cyclic AMP is shown in red, 3'AMP in green, and 5'AMP in blue. Tables show the corresponding B, A, and rate constant values based on color. The reactant, cAMP, was fit with an exponential decay equation ($A \cdot e^{-kt}$) while the products, 5'AMP and 3'AMP, were fit with a quadratic growth equation ($B - A \cdot e^{-kt}$).

Plots with mole percentage versus time are considered to be primary plots. The products, 3'AMP and 5'AMP, were fit with a quadratic growth function (Equation 1). The reactant, cAMP, was fit with an exponential decay function (Equation 2). This allows for rate constant analysis.

One molar NaOH reactions were run with cAMP to have a comparison for the cAMP and Ca^{2+} model system (Figure 20). The different time points from the assay were run on the HPLC. To identify the products, different potential standards, such as adenosine, were run. The chromatographs of the adenosine standard and NaOH cAMP reaction were overlaid for better comparison (Figure 20). Adenosine and adenine production was observed. However, there was much smaller production of adenine since adenosine has to be hydrolyzed to form adenine. A primary plot was also made based on the depletion of cAMP (Figure 21). The rate constant observed from the exponential decay of cAMP was 0.012 hr^{-1} . To understand the difference in catalysis, the rate constants between NaOH and Ca^{2+} catalyzed were compared (Table 1). The NaOH rate was corrected to the pH of 11.5 using the first order dependence on hydroxide. Difference in fold catalysis and $\Delta\Delta G^\ddagger$ were calculated to compare the stabilization of activation energy between the NaOH reactions and Ca^{2+} . These calculations showed an extra 18 kJ/mol stabilization from the Ca^{2+} catalyzed versus NaOH.

To further analyze the role that calcium plays, multiple kinetic assays were run with varying calcium concentrations and analyzed using HPLC. The peaks were integrated and mole percentages were graphed against time in hours to collect the rates

from exponential fits. Rates were also fit from different calcium concentrations with the corresponding calcium concentration for a reaction run at different pH (Figure 22). A

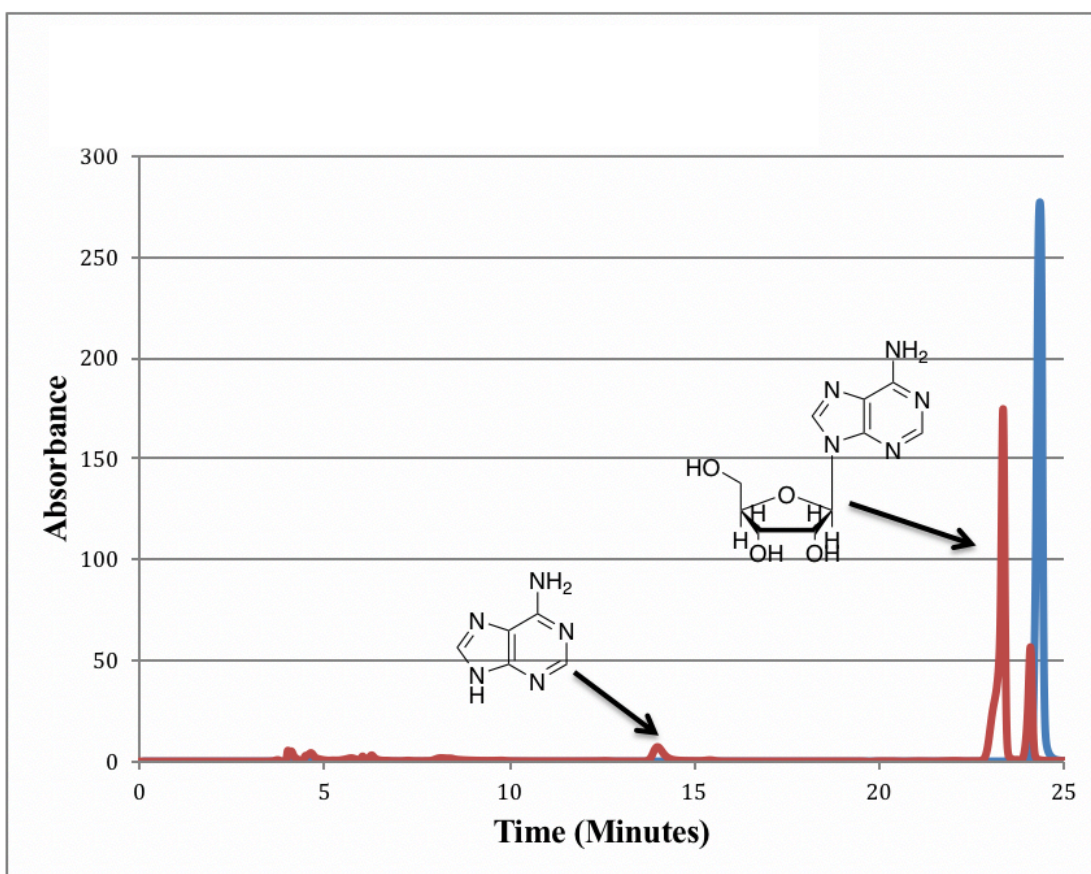


Figure 20. Chromatograph of 1 M NaOH Reaction with cAMP and Adenosine

Standard. Blue shows the adenosine standard and the red is the 24-hour time point of the reaction. An adenosine peak can be seen at approximately 24 minutes, which aligns with the standard, and an adenine peak is seen at approximately 14 minutes. The cAMP peak can be seen at approximately 23 minutes.

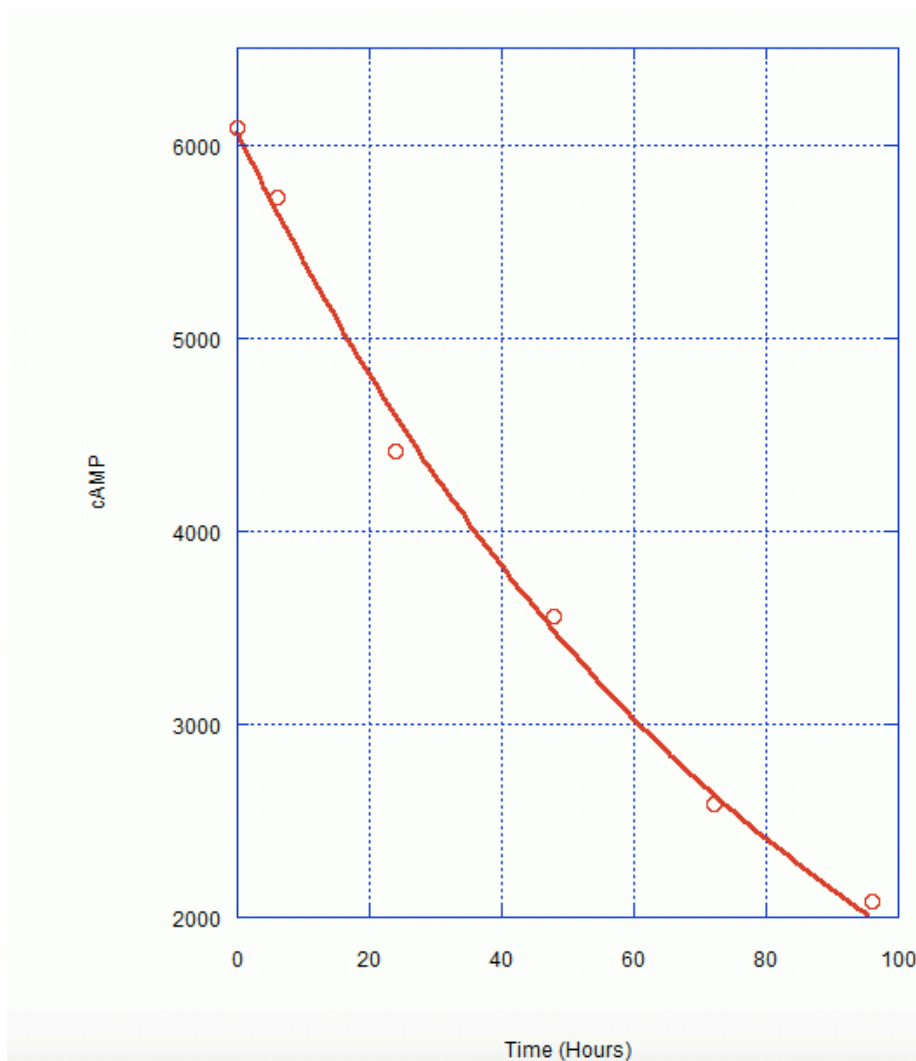


Figure 21. Change in Mole Percentage Over Time for a NaOH Reaction with cAMP.

The reactant, cAMP, was fit with an exponential decay equation ($A \cdot e^{-kt}$).

Conditions	k_{obs} (hr^{-1})	Fold Catalysis	$\Delta\Delta G^\ddagger$ (k J/mol)
1.0 M NaOH	0.012	---	---
Value Corrected to pH 11.5	3.8×10^{-5}	---	---
0.33 M CaCl_2 , pH 11.5	0.031	820	18

Table 1. Calculated $\Delta\Delta G^\ddagger$ of Ca^{2+} Catalyzed versus NaOH

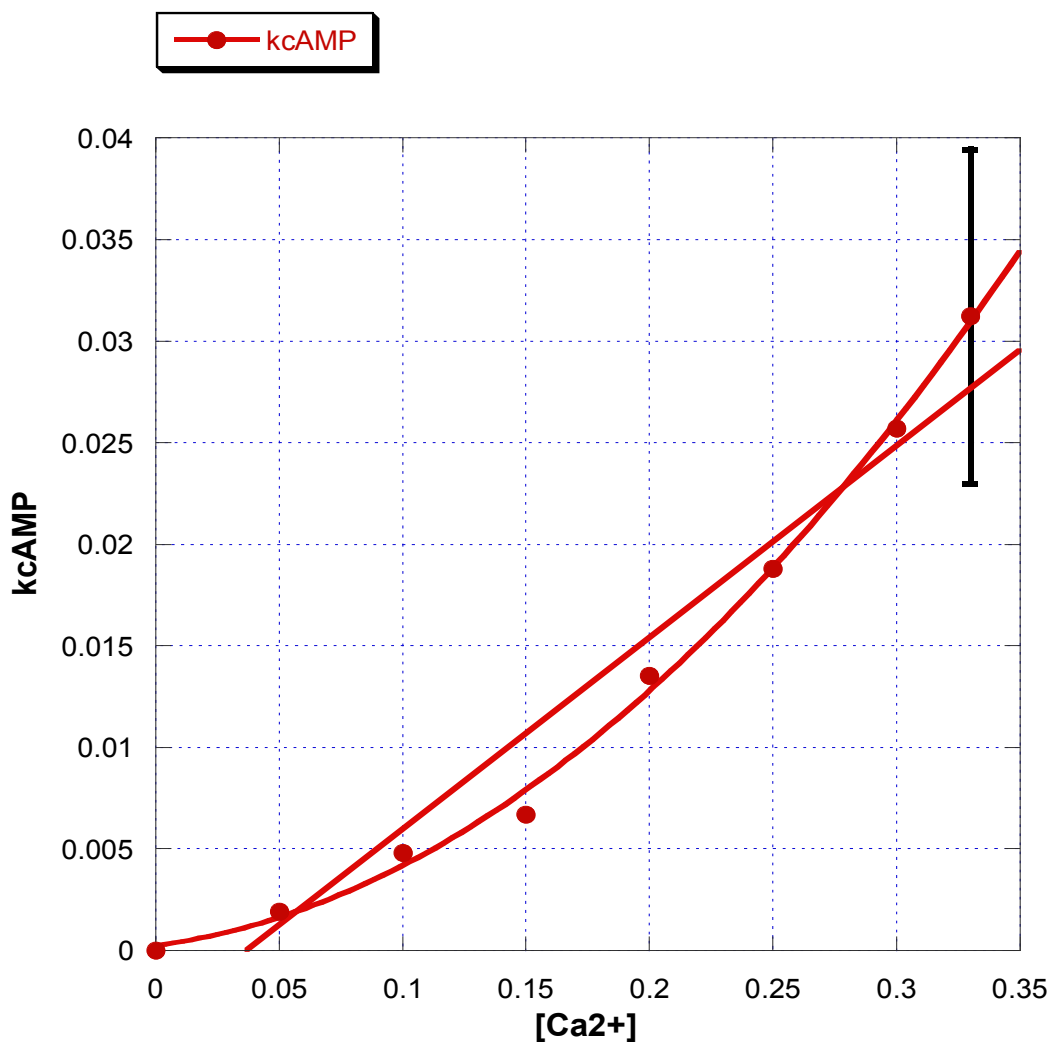


Figure 22. Rate Constant for cAMP Versus [Ca²⁺]. Rate constants were obtained from reactions with different [Ca²⁺]. The rate constant was graphed against the calcium concentration and fit with a quadratic formula ($k_{\text{obs}} = k_0 + k_{1\text{st}} [\text{Ca}^{2+}] + k_{2\text{nd}} [\text{Ca}^{2+}]^2$). A linear fit was also included to show the lack of correlation further supporting the quadratic fit.

quadratic fit was used on the data points, which showed an upward curve (Equation 3). Graphs showing the rates observed versus the Ca^{2+} concentrations are secondary plots. Based on the quadratic fit the following constants were calculated, $k_0 = 2.6 \times 10^{-4} \text{ s}^{-1}$, $k_{1\text{st}}$ is $1.6 \times 10^{-2} \text{ M}^{-1} \text{ s}^{-1}$, and $k_{2\text{nd}}$ is $2.3 \times 10^{-1} \text{ M}^{-2} \text{ s}^{-1}$ where the indicated reaction order is towards Ca^{2+} only. Reactions are pseudo-first order for cAMP with hydroxide concentration unchanged. A linear fit was also included which showed that the data were not a good match to a first order mechanism (Figure 22). A repeat was conducted with multiple concentration of Ca^{2+} but at a lower pH, thus the graphs could not be combined. The secondary plot was fit with an upward curve and $k_0 = 2.6 \times 10^{-4} \text{ s}^{-1}$, $k_{1\text{st}}$ is $1.2 \times 10^{-2} \text{ M}^{-1} \text{ s}^{-1}$, and $k_{2\text{nd}}$ is $3.4 \times 10^{-2} \text{ M}^{-2} \text{ s}^{-1}$ where the indicated reaction order is towards Ca^{2+} only. Reactions are pseudo-first order for cAMP with hydroxide concentration unchanged. Thus, both trials show consistency in the same fit.

Based on the primary plots, it was also observed that at the highest concentration of calcium, the ratio of 3'AMP to 5'AMP was approximately 7:1. To further investigate, the ratios of product formation, 3'AMP:5'AMP, were graphed against the calcium concentrations (Figure 24). The bar graph shows a gradual increase of the ratio, still showing higher 3'AMP production, as the Ca^{2+} concentrations increase. The ratios range from 4:1 to 7:1 when going from 0.05 M Ca^{2+} to 0.33 M Ca^{2+} , indicating Ca^{2+} catalysis favors formation of the 3'-AMP product.

Isotope Assays

Kinetic assays aid in the collection of rate constants and product formation, with respect to differing calcium concentrations. However, to gain a better understanding of the mechanism of hydrolysis by hydroxide attack, isotope reactions were utilized (Figure

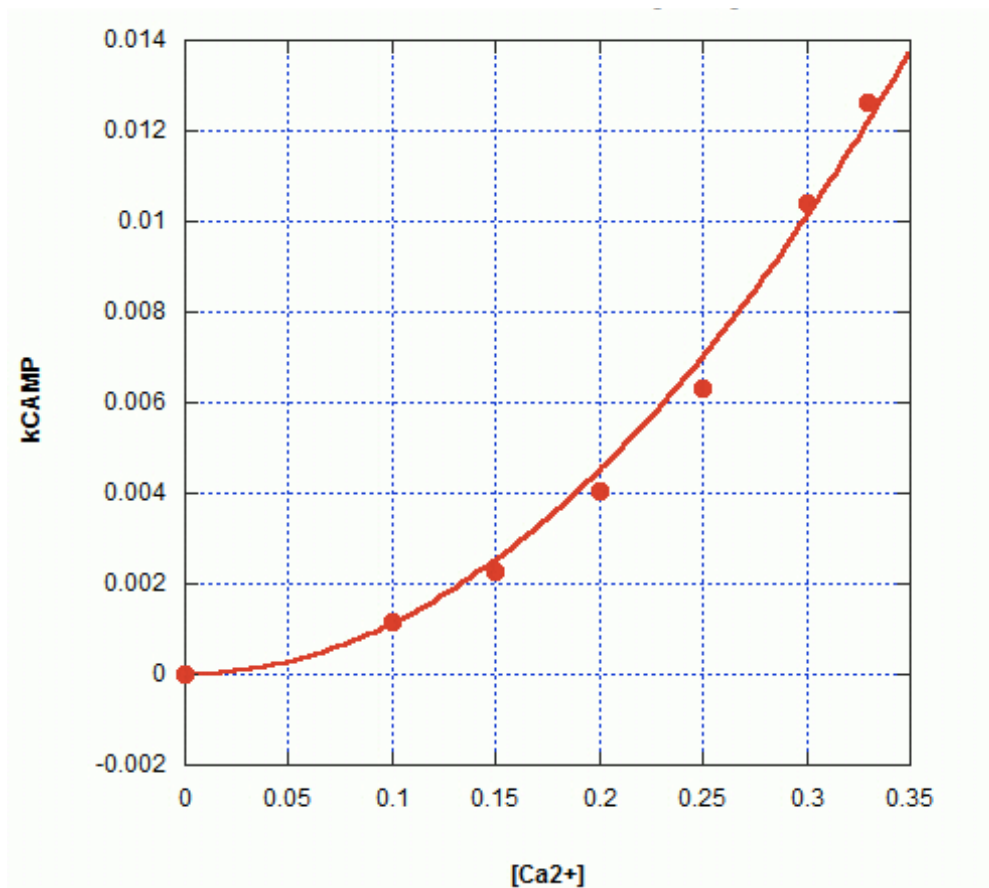


Figure 23. Rate Constant Versus [Ca²⁺] at Lower pH. Rate constants were obtained from reactions with different [Ca²⁺]. The rate constant was graphed against the calcium concentration and fit with a quadratic formula ($k_{\text{obs}} = k_0 + k_{1\text{st}} [\text{Ca}^{2+}] + k_{2\text{nd}} [\text{Ca}^{2+}]^2$).

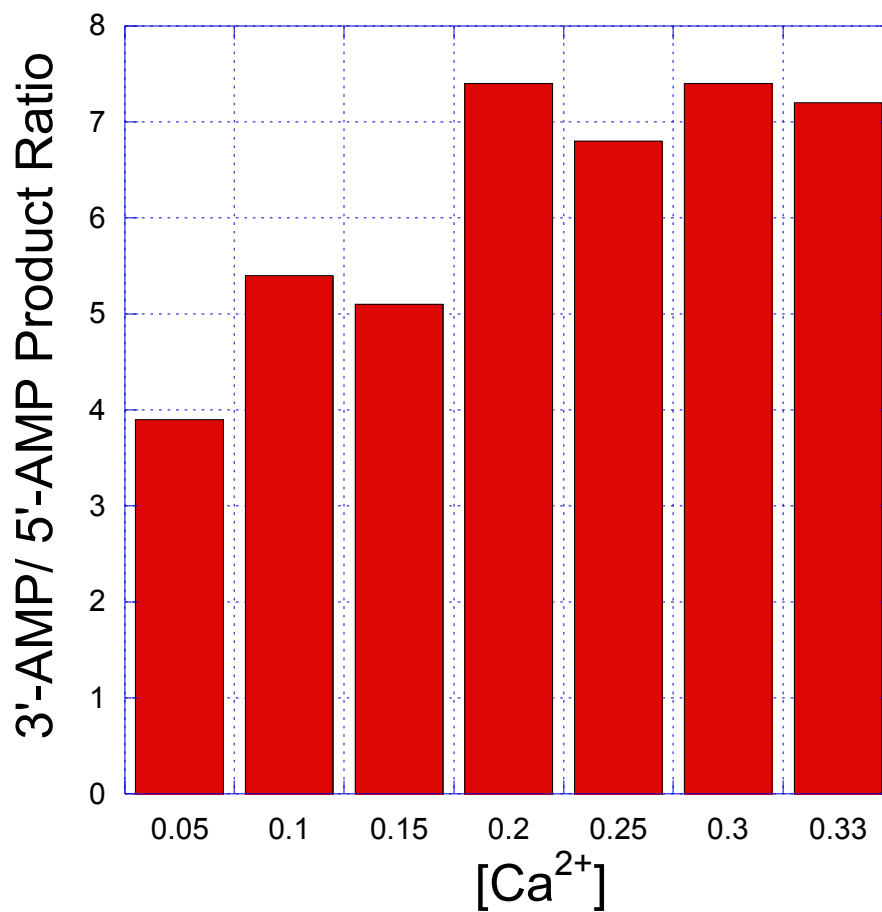


Figure 24. Ca²⁺ Influences the Product Ratio of cAMP Hydrolysis. Product ratios were determined from the A values determined by fitting data for the accumulation of 3'-AMP and 5'-AMP to the equation $y = B - A * e^{-kt}$ as shown in **Figure 19**.

13). Addition of the heavier oxygen atom into 3'AMP and 5'AMP isotope allows for the tracking of the hydroxide attack. We tested whether the metal ion would catalyze the reaction to have hydroxide attack at the phosphorus or the carbon. After the isotope incorporation into 3'AMP and 5'AMP, alkaline phosphatase assays produced adenosine and phosphate. MS analysis of adenosine can show whether the heavier oxygen atom is still incorporated within the molecule. Thus, analysis of the adenosine product by conducting an alkaline phosphatase assay on ^{18}O incorporated 3'AMP and 5'AMP can confirm whether the attack happens at the phosphorus atom or carbon atom.

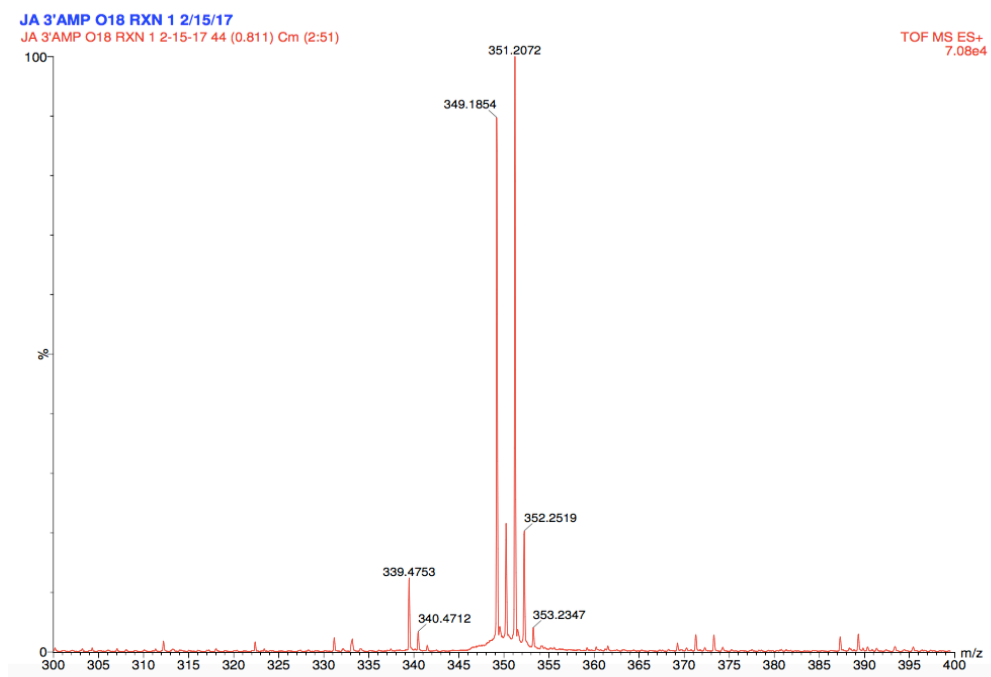
The kinetic assays were run with ^{18}O H_2O as a substitute for ^{16}O H_2O . The reactions ran to maximum time determined from the kinetic assays, and were run on the HPLC to collect the products, 3'AMP and 5'AMP. These samples were dried and then re-suspended before running on the mass spectrometer to confirm incorporation of the isotope (Figure 25). The controls for 3'AMP and 5'AMP showed ^{16}O incorporated samples consistent with a m/z of 349. The 3'AMP mass spectrum showed an m/z of 351 which means that the normal m/z, 349, was shifted over by +2. This is consistent with ^{18}O incorporation considering that ^{18}O is a +2 isotope. The 5' AMP mass spectrum also showed an m/z of 351 showing ^{18}O incorporation considering that the normal m/z is 349 for 5'AMP. The mass spectra showed the isotope incorporation shift, which guarantees that an ^{18}O was assimilated.

The ^{18}O incorporated 5'AMP and 3'AMP were treated with alkaline phosphatase to selectively remove the phosphate group. These samples were run on the HPLC and the

A



B



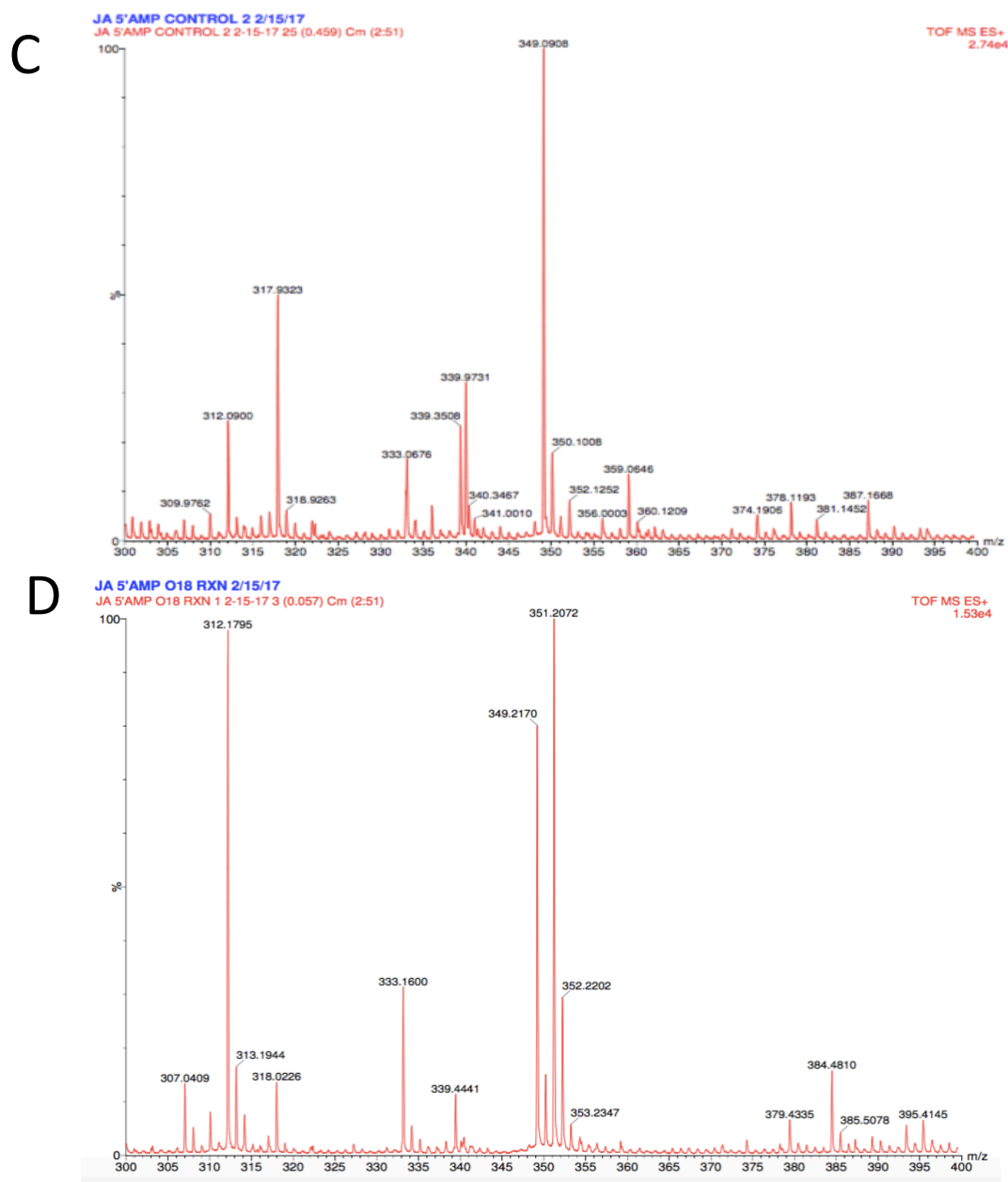


Figure 25. ESI-TOF method mass spectroscopy of ^{18}O isotope incorporated 3' and 5'AMP. A. 3'AMP control spectrum which has a 349 m/z peak B. 3'AMP isotope spectrum which has a 351 m/z peak. C. 5'AMP control spectrum which has a 349 m/z peak. D. 5'AMP isotope spectrum which has a 351 m/z peak.

adenosine peaks were collected. Adenosine samples were dried and run on the mass spectrometer. Adenosine with no ^{18}O incorporation would have a m/z of 268. Thus, if the ^{18}O was still incorporated then there should be a m/z of 270. When analyzing the mass spectrum for the adenosine produced from the ^{18}O incorporated 3'AMP, a m/z of 268 was seen (Figure 26). This is consistent with no ^{18}O incorporation within the adenosine. The mass spectrum for the adenosine produced from the ^{18}O incorporated 5'AMP showed a m/z of 268 which is consistent with no ^{18}O incorporation (Figure 26). Thus, both adenosines only had ^{16}O incorporated. The ^{18}O must have been cleaved with the phosphate group. No incorporation of ^{18}O was seen indicating that attack happened at the phosphorus versus carbon. (Figure 26).

Discussion

Model System Analysis

In the most recent published model system with cAMP and cobalt, the products observed were adenosine and adenine (Chin and Zhou 1987). Neither 3'AMP nor 5'AMP were observed in the cobalt model system (Figure 11). Our experiment with NaOH also showed the inability to record the production of the intermediates, similar to the cobalt model system. Based on the short-lived nature of 3'AMP and 5'AMP, a reaction scheme was proposed by the Cassano laboratory for the rates of intermediate and product formation (Figure 27). The scheme proposes a slow production of 3'AMP and 5'AMP, and a faster production of adenine, adenosine, ribose, and phosphate. This is due to the fact that NaOH reactions show adenosine production by HPLC analysis, but 3'AMP and

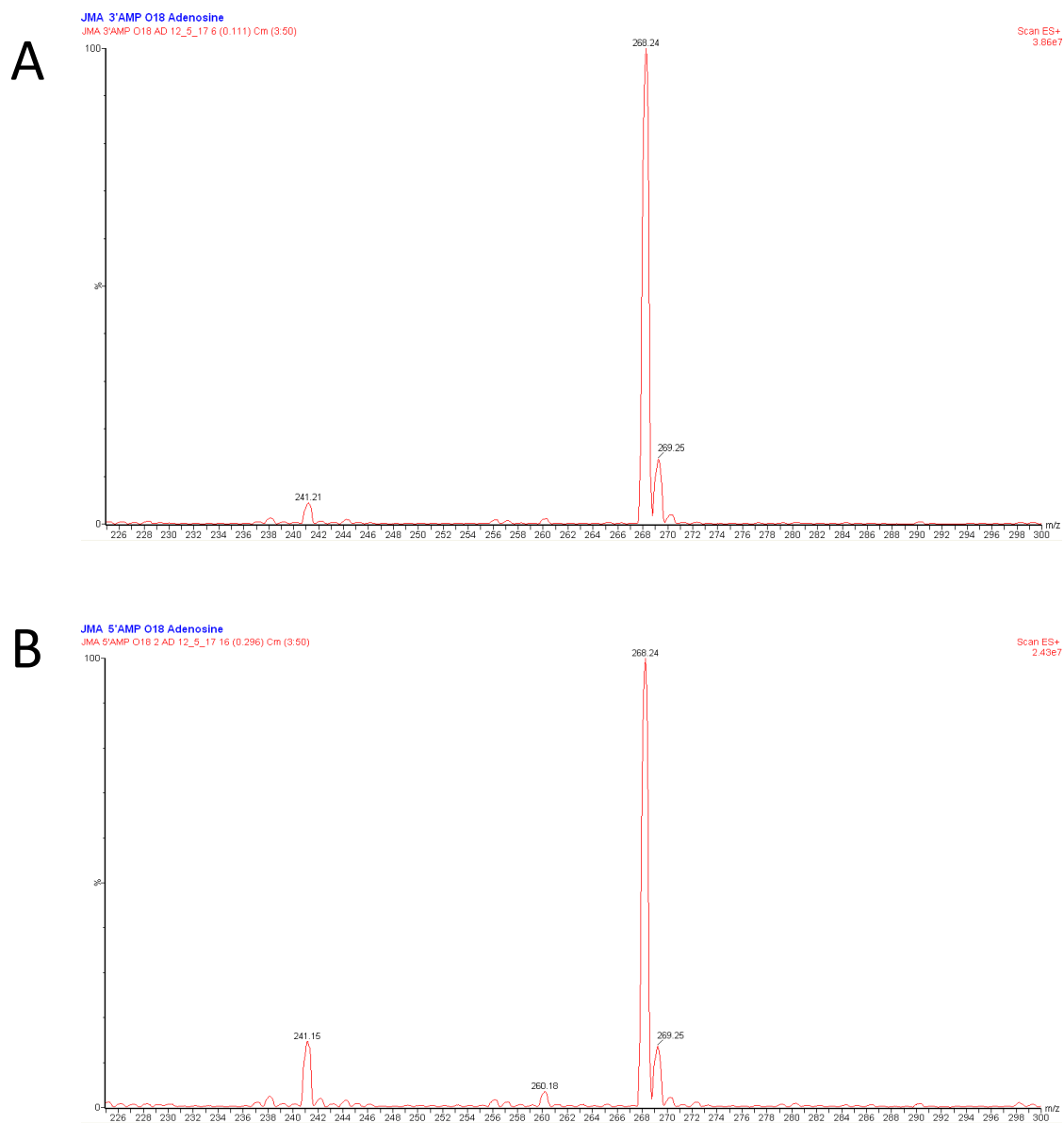


Figure 26. ESI-TOF method mass spectroscopy of Adenosine Derived from ^{18}O isotope incorporated 5'AMP and 3'AMP. A. Spectrum for adenosine derived from 3'AMP, which has a 268 m/z peak. **B.** 5'AMP adenosine spectrum which has a 268 m/z peak.

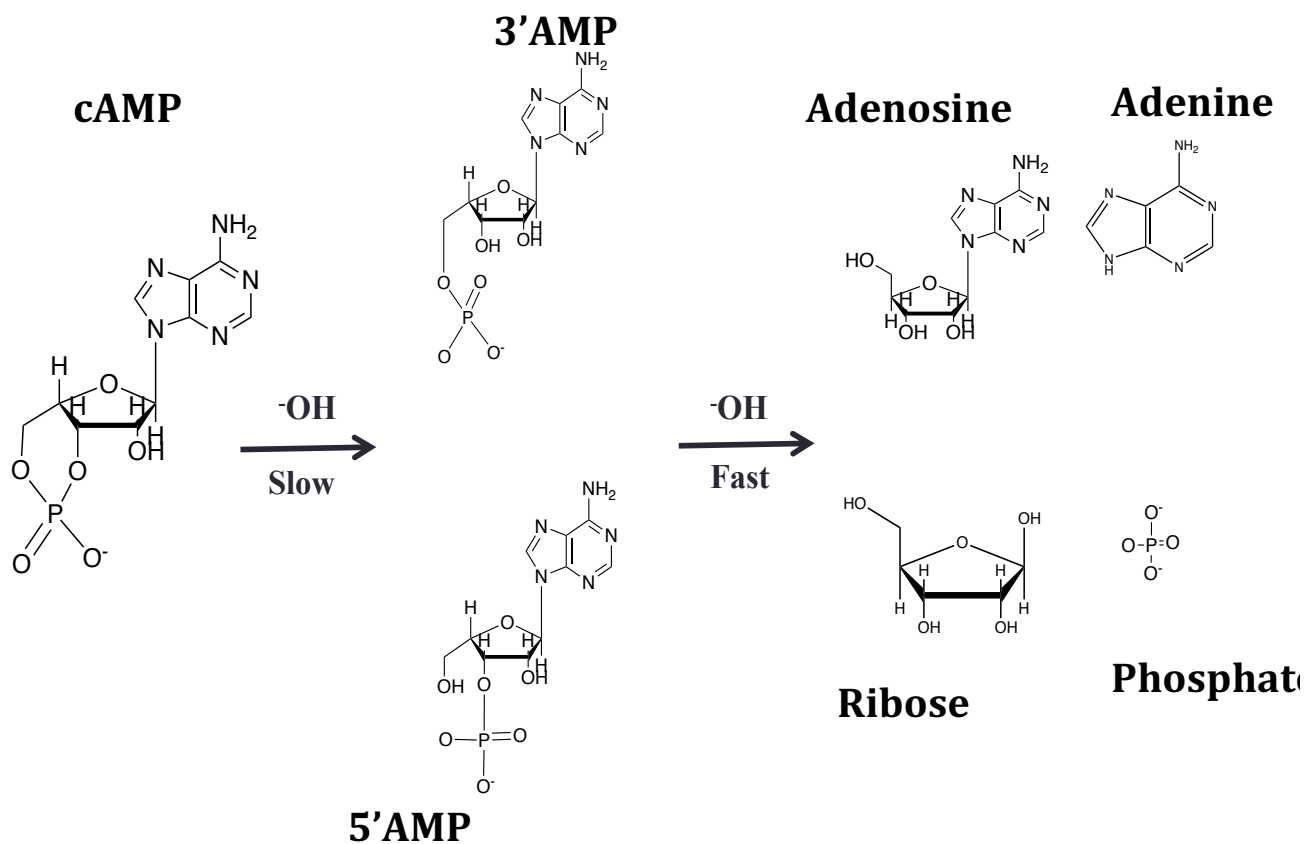


Figure 27. Proposed Reaction Scheme of NaOH Catalyzed Hydrolysis of cAMP

Scheme shows the hydrolysis of cAMP into 3'AMP and 5'AMP to adenosine. Adenosine is slowly hydrolyzed to adenine.

5'AMP cannot be visualized. Thus, the 3'AMP and 5'AMP production must be slow, but the adenosine production fast causing no build up of 3'AMP or 5'AMP. In the model system within this paper, 3'AMP and 5'AMP were identified within the products through HPLC standard analysis and Mass Spectroscopy analysis (Figures 14 and 18). 3'AMP and 5'AMP were also seen within the Ba(OH)₂ model system that showed a ratio of products 4:1 respectively for 3'AMP and 5'AMP (Mehdi et al. 1983).

Mechanistically little is known about the cAMP model system. To investigate the metal ion coordination for catalysis, kinetic assays varying calcium were conducted. The resulting rate constant versus calcium concentration graph gave an upward curve fit (Figure 22 and 23). Observing other model systems, this type of fit is similar to the T5PNP DNA model system (Kirk et al. 2007). Considering that DNA requires the coordination of two metal ions while the RNA model system only required one, it can be hypothesized that a multinuclear mechanism is in place for the cAMP model system.

Comparison with DNA and RNA Models

Initial Cassano laboratory model system comparison between RNA and DNA showed that there is a multinuclear mechanism for DNA cleavage versus single ion mechanism for RNA. We were unsure whether this was due to the poor leaving group or the fact that there is an internal nucleophile for the RNA model system, while the DNA model system has a good leaving group and external nucleophile. The cAMP model has a poor leaving group and an external nucleophile. Based on the secondary plot, the cAMP model system shows the usage of a multinuclear mechanism which is consistent with the DNA model system. Thus, pointing towards the external nucleophile being the common

factor when analyzing the mechanism of metal ions coordinating. To further compare the three models, fold catalysis was calculated from the rate constants comparing NaOH with Ca^{2+} catalyzed (Table 1). Fold catalysis was then compared between the three current model systems within the Cassano laboratory (Table 2). The fold catalysis of cAMP was 820 fold. For the RNA model, UpG the fold catalysis was 326 (Messina 2013). However, the fold catalysis for the DNA model, T5PNP, is 900 which is similar to the cAMP model (Kirk et al. 2007). Thus these similarities in fold catalysis and the multinuclear mechanism correlate to show that the external nucleophile is the distinguishing factor between the model systems. This finding is different from the literature finding for RNA models, where there was higher rate enhancement as the leaving group became worse, showing general acid catalysis (Mikkola et al. 1999). As the leaving group got worse from T5PNP to cAMP, the fold catalysis stayed approximately the same, suggesting catalysis occurs by nucleophilic activation. Moreover, both cAMP and UpG have poor leaving groups, yet their fold catalysis is 820 versus 326, respectively. Thus, the differences in fold catalysis is due to the internal or external nucleophile versus the leaving group.

Molecule	Fold Catalysis
cAMP	820
T5PNP	900
UpG	326

Table 2. Fold Catalysis Comparison Between Model Systems

Product Ratio Analysis

Although data is consistent with a dual ion mechanism, further investigation needs to be conducted as to where these ions are coordinating to create the products 3'AMP and 5'AMP. The surprising factor from the data of mole percentages is that there is an approximate 4 to 7 fold higher amount of 3'AMP produced in comparison to 5'AMP at higher concentrations of calcium (Figure 24). What is the favorable factor that allows for a larger 3'AMP production? A similar ratio was seen in an alkaline hydrolysis which led to a 5:1 ratio of 3'AMP to 5'AMP production (Smith et al. 1960); specifically, 0.2 M barium was used as the catalyst in the Smith and colleagues study. However, Lipkin and colleagues also did the same assay with 0.4 M barium hydroxide and got the same ratio of 5:1 and at double the concentration of metal ion (Lipkin et al. 1959). Specifically with calcium, there is an increased catalytic ability of making 3'AMP as the concentration of metal ion increases. A possible explanation could be that as the concentration of metal ion increases, the metal ion mechanism shifts from a mononuclear mechanism to a multinuclear mechanism. As there are more metal ions available, the preferred route of using two metal ions for catalysis can be taken compared to the one metal ion mechanism. Thus, the ratio increases as the Ca^{2+} increases.

A computational study was conducted on cAMP hydrolysis to analyze the difference in 3'AMP and 5'AMP production (Zhang et al. 2005). When analyzing through Gaussian, a theoretical computational program, with the basis set B3LYP/6-31G**, a non-enzymatic hydrolysis led to 3'AMP being the preferred product. The first step is considered to be the rate limiting step. Energy analysis showed that the reaction

that formed 3'AMP had the smallest ΔE (20.1 kcal/mol) and ΔG (30.4 kcal/mol) compared to 5'AMP which had a ΔE of 22.6 kcal/mol and ΔG of 32.6 kcal/mol. Decreased activation energy, represented by ΔE and ΔG , gives insight into the overall energy of the reaction from reactants to products. These energies are for the first step in the reaction, which was determined to be the limiting step for all the four different reactions they had analyzed. Thus, energetically, it is more favorable to form 3'AMP compared to 5'AMP.

Isotope Analysis

To investigate the mechanism of attack, the isotope assays were conducted. The incorporation of ^{18}O allowed us to track the sites of attack and the mechanism by which each product has formed. The mass spectra confirmed the incorporation of the ^{18}O into 3'AMP and 5'AMP due to the +2 shift of the m/z from 349 to 351 when comparing the control and isotope incorporated (Figure 25). Further analysis conducted with the alkaline phosphatase assays of ^{18}O incorporated 3'AMP and 5'AMP to show that the hydroxide attacks at the phosphorus rather than the carbon (Figure 26). The natural m/z of adenosine is 268 with ^{16}O incorporated, thus if the ^{18}O was incorporated a m/z of 270 would be expected. However, both adenosine samples from 3'AMP and 5'AMP showed m/z peaks of 268. Thus, there is only ^{16}O within the adenosine. The previously incorporated ^{18}O within the 3'AMP and 5'AMP must have been cleaved with the phosphate. This data supports that attack happens at the phosphorus and not at the carbon. This is due to the fact that we do not see ^{18}O incorporation in the adenosine mass

spectrum which implies that the initial incorporation of the ^{18}O hydroxide happened at the phosphorus atom.

This was surprising considering that we expected that attack at the carbon would occur based on aqueous studies that had shown ^{18}O a 100-fold preference for carbon versus the phosphorus (Schroeder 2006). One explanation for this observation can be due to the catalysis caused by calcium. The metal ions could be coordinating in such a manner that it facilitates the attack at the phosphorus by increasing electrophilicity. Another possible reason could be that attack at the carbon is sterically hindered due to the positioning of the calcium ions and the rings' bulkiness.

Future Directions

To analyze this further, two other reactions could be conducted. These include NaOH reactions with H_2^{18}O , and alkaline phosphatase reactions of adenosine monophosphate in H_2^{18}O . The NaOH reactions allow for determining whether the calcium ions are actually catalyzing the attack at the phosphorus considering that in aqueous solution 99% of the time attack happens at the carbon (Schroeder 2006). The alkaline phosphatase reactions will allow for analysis on whether there could be a displacement of the ^{18}O when the phosphate is cleaved. This reaction will serve as a control for the alkaline phosphatase itself. The isotope assay with NaOH adenosine monophosphate will control for the alkaline phosphatase enzyme and ensure that the assay itself is not involved in mis-incorporation of oxygen atoms. To verify the proposed mechanism, further investigation also needs to be conducted on the calcium coordination.

Conclusion

Through the kinetic assays and HPLC analysis, the products of the cAMP and Ca^{2+} model system were shown to be 3'AMP and 5'AMP. The primary and secondary plots gave insight into the multi nuclear mechanism of the metal ions. Isotope assays gave further insight into the hydroxide attack. Single incorporation of the ^{18}O shows that the hydrolysis of cAMP is not an equilibrium reaction. The mass spectra identified that the attack happens at phosphorous possibly due to Ca^{2+} facilitation that makes the phosphorus atom more electrophilic. Based on the kinetic and isotope assays, the cAMP and calcium model system provides data consistent with two calcium ions coordinate to allow for the attack of hydroxide on phosphorus to create products 5'AMP and 3'AMP with a larger ratio of 3'AMP (Figure 27).

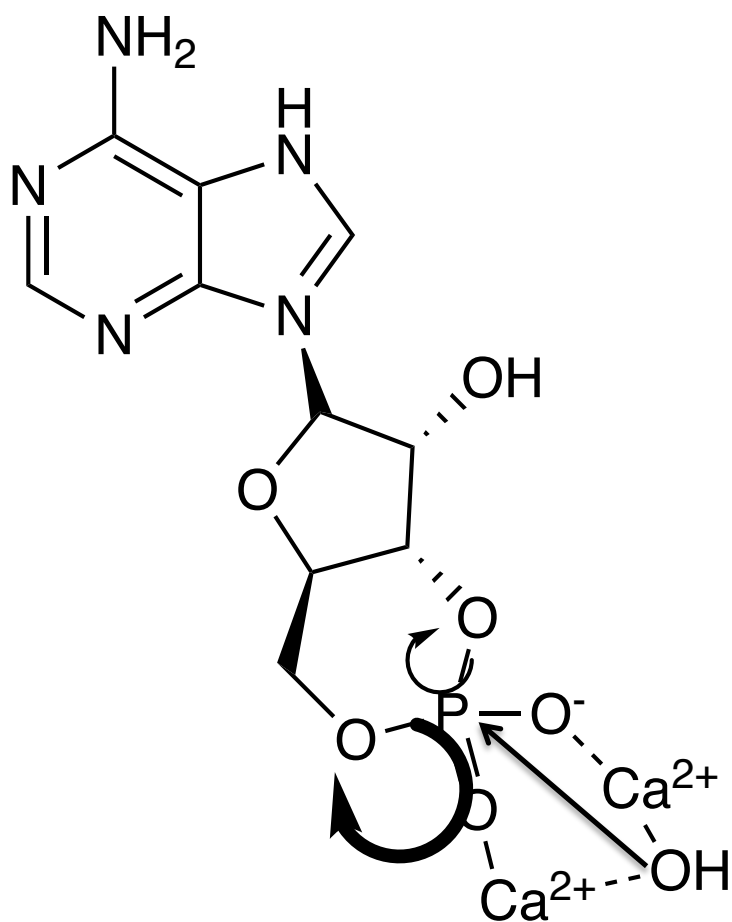


Figure 27. Proposed Reaction of Ca²⁺ Catalyzed Hydrolysis. The hydrolysis of cAMP based on the kinetic and isotope assays with the model system, which shows a slower production of 5'AMP compared to 3'AMP. The thicker arrows represent the higher production of 3'AMP to 5'AMP.

References

- Anderson, V. E., Rusczycky, M. W., Harris, M. E. (2006) Activation of oxygen nucleophiles in enzyme catalysis. *Chem. Rev.* 106, 3236-3251.
- Ariano, M.A., Appleman, M.M. (1979) Biochemical characterization of post-synaptically localized cyclic nucleotide phosphodiesterase. *Brain Res.* 177, 301-309.
- Bonfá, L., Gatos, M., Mancin, F., Tecilla, P., Tonellato, U. (2003) The ligand effect on the hydrolytic reactivity of Zn(II) complexes towards phosphate diesters. *Inorg. Chem.* 42 (12), 3942-3949.
- Bopp, T., Becker, C., Klein, M., Klein-Hebling, S., Palmetshofer, A., Serfling, E., Heib, V., Becker, M., Kubach, J., Schmitt, S., Stoll, S., Schild, H., Staeger, M.S., Stassen, M., Jonuleit, H., Schmitt, E. (2007) Cyclic adenosine monophosphate is a key component of regulatory T cell-mediated suppression. *Journal of Experimental Medicine* 204 (6), 1303-1310.
- Breer, H., Shepherd, G.M. (1993) Implications of the NO/cGMP system for olfaction. *Trends in Neuroscience* 16 (1), 5-9.
- Buettner, M. J., Spitz, E., Rickenberg, H.V. (1973) Cyclic adenosine 3',5'-monophosphate in *Escherichia coli*. *J. Bacteriol* 114 (3), 1068-1973.
- Bunton, C. A., Llewellyn D.R., Oldham K. G., Vernon C. A. (1958) The reactions of organic phosphates. 1 The hydrolysis of methyl dihydrogen phosphate. *J. Chem. Soc.* 3574-3587.
- Carter, A. J., Ballard, S. A., Naylor, A. M. (1998) Effect of the selective phosphodiesterase type 5 inhibitor sildenafil on erectile dysfunction in the anesthetized dog. *The Journal of Urology* 160 (1), 242-246.
- Chin J, Zhou X. (1987) Catalytic hydrolysis of cAMP. *Canadian Journal of Chemistry*, 65 (8), 1882-1884.
- Christian, E.L., Anderson, V.E., Carey, P.R., Harris, M.E. (2010). A Quantitative Raman Spectroscopic Signal for Metal– Phosphodiester Interactions in Solution. *Biochemistry* 49(13), 2869-2879.
- Corbin, J. D., Francis, S. H. (2002) Pharmacology of phosphodiesterase-5 inhibitors. *International Journal of Clinical Practice* 56 (6), 453-459.

- Feldman, M. D., Copelas, L., Gwathmey, J. K., Phillips, P., Warren, S. E., Schoen, F. J., Grossman, W., Morgan, J. P. (1987) Deficient production of cyclic AMP: pharmacologic evidence of an important cause of contractile dysfunction in patients with end-stage heart failure. *Circulation* 75, 331-339.
- Ferscht, A. *Enzyme structure and mechanism*; Freeman: New York, NY, 1999.
- Gerlt, J.A., Westheimer, F.H., Sturtevant, J.M. (1974) The Enthalpies of Hydrolysis of Acyclic, Monocyclic, and Glycoside Cyclic Phosphate Diesters. *The Journal of Biological Chemistry* 250 (13), 5059-5067.
- Halpin, D. M. G. (2008) ABCD of the phosphodiesterase family: interaction and differential activity in COPD. *Int. J. Chron. Obstruct Pulmon. Dis.* 3 (4), 543-561.
- Hamblin, N. J., Angell, T.D.R., Ballantine, S.P., Cook, C.M., Cooper, A.W.J., Dawson, J., Delves, C.J., Jones, P.S., Linnvall, M., Lucas, F.S., Mitchell, C.J., Neu, M.Y., Ranshaw, L.E., Solanke, Y.E., Somers, D.O., Wiseman, J.O. (2008) P yrazolopyridines as a novel structural class of potent and selective PDE inhibitors. *Bioorganic & Medicinal Chemistry Letters* 14, 4237-4241.
- Huai Q., Colicelli J., Ke H. (2003) The Crystal Structure of AMP-Bound PDE4 Suggests a Mechanism for Phosphodiesterase Catalysis. *Biochemistry* 42, 13220-13226.
- Hurst, P., Takasaki, B.K., Chin, J. (1996) Rapid Cleavage of RNA with a La(III) Dimer. *J. Am. Chem. Soc.* 118, 9982-9983.
- Kirk, B.A., Cusack, C.L., Laager, E., Rochlis, E., Thomas, T., Cassano, A.G. (2007) Mononuclear and dinuclear mechanisms for catalysis of phosphodiester cleavage by alkaline earth metal ions in aqueous solution. *Journal of Inorganic Biochemistry*, 10, 207-210.
- Korhonen, H., Koivusalo, T., Toivola, S., Mikkola, S. (2013) There is no universal mechanism for the cleavage of RNA model compounds in the presence of metal ion catalysts. *Org. Biomol. Chem.* 11, 8324-8339.
- Lasilla, J. K., Zalatan, J. G., Herschlag, D. (2011) Biological phosphoryl-transfer reactions: understanding mechanism and catalysis. *Annu. Rev. Biochem.* 80, 669-702
- Lehninger, A. L. (1950) Role of metal ions in enzyme systems. *American Physiology Society* 30, 393-429.
- Lipkin, D., Cook, W.H., Markham, R. (1959) Adenosine-3' :5'-phosphoric Acid: A Proof

of Structure. *J. Am. Chem. Soc.* 81, 6198-6203.

Mehdi, S., Coderre, J.A., Gerlt, J.A. (1982) Stereochemical Course of the Base-Catalyzed Hydrolysis of Cyclic 2'-Deoxyadenosine 3',5'-[¹⁷O, ¹⁸O]Monophosphate. *Tetrahedron* 39(21), 3483-3492.

Messina, K. (2013) **Investigation of the Mechanism of Ca²⁺ Catalyzed RNA Phosphodiester Hydrolysis** Drew University.

Mikkola, S., Stenman, E., Nurmi, K., Yousefi-Salakdeh, E., Strömberg, R., Lönnberg, H. (1999) The mechanism of the metal ion promoted cleavage of RNA phosphodiester bonds involves a general acid catalysis by the metal aquo ion on the departure of the leaving group. *J. Chem. Soc.* 2, 1619-1625.

Nicholson, D. C., Challiss, J. R. A., Shahid, M. (1991) Differential modulation of tissue function and therapeutic potential of selective inhibitors of cyclic nucleotide phosphodiesterase isoenzymes. *Trends in Pharmacological Sciences* 12, 19-27.

Ora, M., Peltomäki, M., Oivanen, M., Lönnberg, H. (1998) Metal-Ion-Promoted Cleavage, Isomerization, and Desulfurization of the Diastereomeric Phosphoromonothioate Analogues of Uridylyl(3',5')uridine. *J. Org. Chem.* 63, 2939-2947.

Paller, A.S., Tom, W.L., Lebwohl, M.G., Blumenthal, R.L., Boguniewicz, M., Call, R.S., Eichenfield, L.F., Forsha, D.W., Rees, W.C., Simpson, E.L., Spellman, M.C., Stein Gold, L.F., Zaenglein, A.L., Hughes, M.H., Zane, L.T., Hebert, A.A. (2016) Efficacy and safety of crisaborole ointment, a novel, nonsteroidal phosphodiesterase 4 (PDE4) inhibitor for the topical treatment of atopic dermatitis (AD) in children and adults. *J. Am. Acad. Dermatol.* 3, 494-503.

Pastan, I., Perlman, R. (1970) Cyclic adenosine monophosphate in bacteria. *Science* 169 (3943), 339-344.

Roigk, A., Hettich, R., Schneider, H. (1997) Unusual Catalyst Concentration Effects in the Hydrolysis of Phenyl Phosphate Esters and of DNA: A Systematic Investigation of the Lanthanide Series. *Inorg. Chem.* 37, 751-756.

Schramm, V. L. (1998) Enzymatic transition states and transition state analog design. *Annual Review of Biochemistry* 67, 693-720.

Schroeder, G. K., Lad, C., Wyman, P., Willaims, N.H., Wolfenden, R. (2006). The time required for water attack at the phosphorus atom of simple phosphodiester and of DNA. *PNAS* 103 (11), 4052-4055.

- Serezani, C.H., Ballinger, M.N., Aronoff, D.M., Peters-Golden, M. (2008). Cyclic AMP-Master Regulator of Innate Immune Cell Function. *Am. J. Respir. Cell Mol. Biol.* 39, 127-132.
- Smith, M., Drummond, G. I., Khorana, H.G. (1960) Cyclic Phosphates. IV. Ribonucleoside-3', 5' Cyclic Phosphates. A General Method of Synthesis and Some Properties. *J. Am. Chem. Soc.* 83, 698-706.
- Soderling, S. H., Beavo, J.A. (2000) Regulation of cAMP and cGMP signaling: new phosphodiesterases and new functions. *Current Opinion in Cell Biology* 12, 174-179.
- Sutherland, E. W. (1970) On the Biological Role of Cyclic AMP. *JAMA* 214 (7), 1281-1288.
- Wehbi, V. L., Taskén, K. (2016) Molecular mechanisms for cAMP-mediated immunoregulation in T cells- role of anchored protein kinase A signaling units. *Front Immunol.* 7, 222.
- Westheimer, F.H. (1987) Why nature chose phosphates. *Science* 235, 1173-1178.
- Williams, N.H., Wyman P. (2001) Base catalysed phosphate diester hydrolysis. *The Royal Society of Chemistry* 0, 1268-1269.
- Zhang, A., Liu, K., Wang, C., Ma, S., Li, Z. (2005) Theoretical study on the ring-opening hydrolysis reaction of cAMP. *Journal of Molecular Structure* 719, 149-152.